Hadron masses with two quark flavors

Steven Gottlieb
Department of Physics, Indiana University, Bloomington, Indiana 47405

W. Liu
Department of Physics, University of California, La Jolla, California 92093

R. L. Renken and R. L. Sugar
Department of Physics, University of California, Santa Barbara, California 93106

D. Toussaint
Fermi National Accelerator Laboratory, P.O. Box 500, Batavia, Illinois 60510
and Department of Physics, University of California, La Jolla, California 92093
(Received 26 May 1988)

We investigate the hadron mass spectrum in lattice QCD with two flavors of dynamical quarks. We use $6^3\times 24$, $8^3\times 24$, and $10^3\times 24$ lattices with $6/g^2$ adjusted so that the thermal crossover temperature is $1/4a$ or $1/6a$. At these values of $6/g^2$ flavor symmetry is not restored and the familiar problem of the nucleon to ρ mass ratio is not fixed by the dynamical fermions. For comparison and checking we measure the spectrum in the quenched approximation using analogous couplings and identical methods. The effects of the finite spatial size are investigated and found to be small. We discuss our fitting procedures and our control of systematic errors in some detail. We combine our mass measurements with previous calculations to estimate the temperature for the transition to a chirally symmetric phase of QCD in physical units.

I. INTRODUCTION

The advent of stochastic simulation techniques[1] in lattice gauge theory has raised the tantalizing prospect of computing the masses of the hadrons[2] from first principles. Eventually coupling constants,[3] wave functions,[4] and weak decay amplitudes[5] as well as masses should be calculable. In practice, these computations[6] are proving to be more difficult than early optimistic estimates suggested. Nevertheless, a numerical computation of the hadron spectrum would be a dramatic test of QCD and might well lead to a better understanding of QCD at low energies.

We have performed a moderately large simulation of the lattice QCD with two flavors of dynamical quarks using the Kogut-Susskind formulation of lattice fermions with lattices as large as $10^3\times 24$. Our simulation uses quark masses of 0.1, 0.05, and 0.025, which are larger than the real world u- and d-quark masses. Although we are not in the continuum limit, as evidenced by the fact that flavor symmetry[7] is not restored, it is still interesting to compare our results with quenched approximation calculations. We also did a small spectrum calculation without dynamical fermions on the same size lattice and at the corresponding value of $6/g^2$ to compare with the dynamical fermion calculation. Of course, much larger quenched spectrum calculations have been done,[8] but it is interesting to compare to a similar quenched calculation using exactly the same fitting procedures and to test our procedures by comparing our pure gauge QCD results to other quenched approximation results. Further, using our mass estimates to set the mass scale allows us to estimate the temperature of chiral-symmetry restoration in MeV (Ref. 9). This last number is interesting for the physics of the early Universe and for relativistic heavy-ion collisions.

In principle, the only inputs to a lattice calculation are the quark mass and the strong-coupling constant. In practice, there are a number of other parameters which must be set and extrapolations must be made in the mass and coupling to approach the physical limit. The reliability of any simulation can only be judged with detailed knowledge of how these parameters are set and how the extrapolation is done. Thus, before we discuss the physical interpretation of our results, we give a thorough discussion of how we attempted to control systematic biases arising from our choice of parameters. Section II of this paper presents basic notation, a discussion of the propagators we measure, and how they are fit to determine particle masses. In Sec. III we discuss the parameters of the simulation and our attempts to control systematic errors. Section IV contains our discussion of the particle masses given the caveats of Sec. III. Section V is devoted to our estimate of the crossover temperature for the transition to a chirally symmetric phase of QCD. Finally, Sec. VI contains our conclusions.

II. NOTATION AND PROPAGATOR FITTING

We use two flavors of dynamical staggered quarks in our simulation, using the version of the hybrid-molecular-dynamics method[10] described in our earlier

work.[11] This method allows us to vary the number of quark flavors while keeping the systematic errors due to the finite size Δt of the molecular-dynamics steps of order $(\Delta t)^2$. We generate gauge-field configurations with probability

$$P(U)=\frac{1}{Z}(\det M)^{N_f/4}\exp(-S_g)\ , \tag{1}$$

where S_g is the Wilson action for the gauge fields and M is the Kogut-Susskind hopping matrix describing four flavors of quarks:

$$M_{x,y}=2m\delta_{x,y}+\sum_{\mu}\eta_{x,\mu}(U_{x,\mu}\delta_{x,y-\mu}-U^{\dagger}_{x-\mu,\mu}\delta_{x,y+\mu})\ , \tag{2}$$

where x and y denote lattice sites and we have suppressed the color indices. The use of a fractional power of the determinant, which is common practice,[12] weights each internal fermion loop by a factor of $N_f/4$ as is appropriate for N_f flavors. However, the hadronic correlation functions that we measure still have four flavors of valence quarks. Thus, if we had flavor symmetry we would expect that symmetry to be SU(4) rather than SU(2). Since the quark loops are weighted for N_f flavors, we obtain hadron masses corresponding to that number. Once the gauge configuration is generated the method of measuring hadron propagators is independent of the number of flavors or the quark mass used in generating the configuration.

Our hadron propagator measurements are completely conventional.[13] After calculating the inverse of the hopping matrix in Eq. (2), we construct zero-momentum hadron propagators as follows: local meson propagators as a function of time are given by

$$P_M(t)=\sum_{\mathbf{x}}\sum_{ij}W_M(\mathbf{x})M^{-1}(\mathbf{0},0,i;\mathbf{x},t,j)\times M^{-1}(\mathbf{x},\mathrm{t},\mathrm{j};\mathbf{0},0,\mathrm{i})\ , \tag{3}$$

where i and j are color indices, $(\mathbf{0},0)$ is the source point, $(\mathbf{x},t)$ is the sink point, and W_M is a weighting factor which picks out a meson state with particular symmetry properties. In this context "local" means created by a quark-antiquark operator on a single lattice site. For completeness we tabulate the weighting factors in Table I. Each propagator contains particles of both parities, and the particle interpretation for each propagator is also listed in Table I. It is convenient to refer to the channels as pseudoscalar (PS), vector tensor (VT), pseudovector (PV), and scalar (S) (Ref. 14). The easiest channels to measure for the π and ρ mesons are PS and VT, respectively. Because particles of both parities appear in each propagator, we also find the π and ρ mesons in S and PV, respectively. We will use the notation π_2 and ρ_2 to refer to properties of the π and ρ measured in these channels.

The most general function we use to fit the propagators includes terms for the two lowest states of each parity. The terms below that oscillate in t correspond to opposite-parity particles. For the zero-momentum meson propagators we use

$$\begin{aligned}P_M(t)=&Ae^{-mt}+Ae^{-m(T-t)}\\&+(-1)^t\tilde{A}e^{-\tilde{m}t}+(-1)^t\tilde{A}e^{-\tilde{m}(T-t)}\\&+A^*e^{-m^*t}+A^*e^{-m^*(T-t)}\\&+(-1)^t\tilde{A}^*e^{-\tilde{m}^*t}+(-1)^t\tilde{A}^*e^{-\tilde{m}^*(T-t)}\ ,\end{aligned} \tag{4}$$

where a tilde indicates opposite parity and an asterisk indicates an excited state, T is the length of the lattice in the time direction, and t is the distance from the source (Euclidean time). The nucleon propagator is similar, but takes into account the antiperiodic boundary conditions in Euclidean time and the fact that the particles whose propagators alternate in the forward direction do not alternate in the backward direction:

$$\begin{aligned}P_B(t)=&Ae^{-mt}-(-1)^tAe^{-m(T-t)}\\&+(-1)^t\tilde{A}e^{-\tilde{m}t}-\tilde{A}e^{-\tilde{m}(T-t)}\\&+A^*e^{-m^*t}-(-1)^tA^*e^{-m^*(T-t)}\\&+(-1)^t\tilde{A}^*e^{-\tilde{m}^*t}-\tilde{A}^*e^{-\tilde{m}^*(T-t)}\ .\end{aligned} \tag{5}$$

In most of the fits we did not use all of the parameters in Eqs. (4) or (5). We have used fits containing from one to four particles, or two to eight parameters.

The fitting is performed using a least-squares procedure that takes into account the fact that the propagator values at different distances from the source are correlated. We will present our fitting method in some detail. The logic is standard and has been used before in lattice gauge calculations,[15] but we wish to be clear about our methods and, hopefully, useful to others who may wish to do these studies.

Before confronting the correlations of propagator averages at different distances, we must deal with correlations of measurements in simulation time. Let x_k be the kth measurement of a quantity. Successive measurements are not statistically independent, and their autocorrelation is measured by the fractional autocorrelation at simulation time separation j:

TABLE I. The weight vectors used in the construction of local meson propagators and the particle interpretation for the corresponding propagator.

Channel	$W_M(x,y,z)$	Part. interp.	Opp. parity
PS	1	π	ϵ
VT	$(-1)^x+(-1)^y+(-1)^z$	ρ	b_1
PV	$(-1)^{y+z}+(-1)^{x+z}+(-1)^{x+y}$	ρ_2	a_1
S	$(-1)^{x+y+z}$	π_2	σ

$$C_j = \frac{\langle x_k x_{k+j} \rangle - \langle x_k \rangle^2}{\langle x_k^2 \rangle - \langle x_k \rangle^2} . \quad (6)$$

In order to reduce the effect of the autocorrelations it is customary to "block," or average several successive measurements, and treat the block averages as independent. If Y_k is the average over the kth block, then the variance of the block averages is

$$\langle Y_k^2 \rangle - \langle Y_k \rangle^2 = \frac{\langle x_j^2 \rangle - \langle x_j \rangle^2}{N_b} \left[1 + 2 \sum_{i=1}^{N_b - 1} C_i \right] , \quad (7)$$

where N_b is the number of measurements in each block. Ideally N_b should be large enough to saturate the quantity in parentheses in Eq. (7). It is notoriously difficult to measure the C_j directly. If the autocorrelation is measured in an uncorrelated sequence of M numbers, the result will fluctuate by $1/\sqrt{M}$, making correlations smaller than this unobservable. In general, we expect the autocorrelation to be a sum of exponentials with varying amplitudes. It is easy to see that a slow decay with small amplitude can escape detection in measuring the C_j. Thus the block sizes N_b should be made large. However, in the following analysis it is important to have a reasonable number of blocks, so we have not made N_b as large as we would like. In a more extensive simulation it would be desirable to increase N_b. We will present empirical results for the autocorrelation of our measurements later.

In our analysis for all propagators except the π (PS) we average five successive propagator measurements taken over ten simulation time units to obtain each block average. For the π in our weaker coupling runs ($aT_c = \frac{1}{6}$) we block together ten successive measurements, or 20 time units, which results in an increase of about 15% in the apparent statistical errors in the π mass as compared with blocking five measurements. Further increasing the block size to 20 increases the errors on the pion mass by another 10%, but leaves us with uncomfortably few blocks. For the pions in our stronger coupling runs ($aT_c = \frac{1}{4}$) and for the other propagators, which have much larger fluctuations, we see no effect from increasing the block size from five to ten. For most of our runs we have 500 propagators and the number of blocks N is equal to 50 for the π (PS) and to 100 for the other particles. (See Table II for a summary.)

After blocking we have N blocks of propagator measurements, with the blocks now assumed to be independent. We denote the kth block at distance i by Y_{ki}, the average over these N blocks by $\bar{Y}_i$, and the true value or average over an infinite number of measurements by $\bar{\bar{Y}}_i$. We assume that the measured values of $\bar{Y}_i$ have a Gaussian probability distribution $P(\{\bar{Y}\})$ about the true value:

$$P(\{\bar{Y}\}) = Z^{-1} \exp[-\tfrac{1}{2} (\bar{Y}_i - \bar{\bar{Y}}_i)(C^{-1})_{ij} (\bar{Y}_j - \bar{\bar{Y}}_j)] , \quad (8)$$

where C_{ij} is the covariance matrix of the $\bar{Y}_i$ and

$$Z = \int [d\bar{Y}] \exp[-\tfrac{1}{2} (\bar{Y}_i - \bar{\bar{Y}}_i)(C^{-1})_{ij} (\bar{Y}_j - \bar{\bar{Y}}_j)] . \quad (9)$$

(A naive fitting method amounts to setting the off-diagonal elements of C_{ij} to zero. We find relative correlations as large as 0.997 among pion-propagator measurements at adjacent distances, and 0.989 among measurements four time slices apart.) Notice that it is the average $\bar{Y}_i$ rather than the individual blocks of propagators Y_{ki} which is assumed to have a Gaussian distribution. As we shall see later, the distributions of the Y_{ki} are far from Gaussian. The covariance matrix is estimated from the measurements:

$$C_{ij} = \frac{1}{N-1} \left[\frac{1}{N} \sum_{k=1}^{N} Y_{ki} Y_{kj} - \bar{Y}_i \bar{Y}_j \right] . \quad (10)$$

TABLE II. This table summarizes the parameters of the various runs. The first column gives the temperature and the lattice size. am_q is the mass of the quark, dt is the microcanonical time step, N_T is the number of trajectories made during the run, n_u is the number of conjugate-gradient iterations required during an updating step, N_P is the number of propagator measurements made during the run, and n_m is the number of conjugate-gradient iterations required to make a measurement. Each run also included an additional 100 warm-up trajectories.

	am_q	$6/g^2$	dt	N_T	n_u	N_P	n_m
$aT_c = \frac{1}{4}$	0.1	5.375	0.04	1000	54	200	87
$6^3 \times 24$	0.05	5.32	0.04	1000	92	200	160
	0.025	5.2875	0.02	1000	151	250	333
$aT_c = \frac{1}{4}$	0.1	5.375	0.04	1000	54	500	96
$8^3 \times 24$	0.05	5.32	0.04	1000	93	500	175
	0.025	5.2875	0.02	1000	152	500	338
$aT_c = \frac{1}{6}$	0.1	5.525	0.04	1000	50	500	92
$8^3 \times 24$	0.05	5.47	0.04	1000	83	500	167
	0.025	5.4375	0.02	1000	131	500	311
$aT_c = \frac{1}{6}$	0.1	5.525	0.04	1000	51	500	92
$10^3 \times 24$	0.05	5.47	0.04	1000	83	500	166
	0.025	5.4375	0.02	1000	131	500	311
$aT_c = \frac{1}{6}$	0.05	5.865	0.05	400		200	154
$10^3 \times 24$ quenched	0.025	5.865	0.05	500		250	283

The matrix C_{ij} is a positive-definite quadratic form. If we have a theory for $\bar{\bar{Y}}$ (e.g., that the zero spatial momentum propagator fits to a sum of exponentials), then we assume

$$\bar{\bar{Y}}_i = f_i(\lambda_1, \ldots, \lambda_n) \tag{11}$$

and we want to choose the parameters λ_a to give the best fit. We will denote the parameters determined in our experiment as $\bar{\lambda}_a$ and the parameters one would obtain from an infinitely long run as $\bar{\bar{\lambda}}_a$. The best fit is defined by maximizing the probability of getting the experimental result $\bar{Y}_i$, i.e., by minimizing

$$\chi^2 = [\bar{Y}_i - f_i(\bar{\lambda})](C^{-1})_{ij}[\bar{Y}_j - f_j(\bar{\lambda})] \tag{12}$$

with respect to the $\bar{\lambda}_a$. So, to find the best fit we solve

$$\frac{\partial \chi^2}{\partial \bar{\lambda}_a} = 0 = 2\frac{\partial f_i(\lambda)}{\partial \bar{\lambda}_a} C_{ij}^{-1}[f_j(\bar{\lambda}) - \bar{Y}_j] \ . \tag{13}$$

This minimization condition gives different values for the parameters as well as different errors on the parameters than a fit which ignores the correlations. As an amusing note, it is possible (and in fact happens in some of our pion fits) that the best fit of the form $A(e^{-mt} + e^{m(T-t)})$ falls below the average propagator at every distance.

We use a modified Newton's method to perform the minimization, so we also compute the Hessian

$$\begin{aligned} H_{ab} &= \frac{\partial^2 \chi^2}{\partial \lambda_a \partial \bar{\lambda}_b} \\ &= 2\frac{\partial^2 f_i(\lambda)}{\partial \bar{\lambda}_a \partial \bar{\lambda}_b} C_{ij}^{-1}[f_j(\bar{\lambda}) - \bar{Y}_j] \\ &\quad + 2\frac{\partial f_i(\lambda)}{\partial \bar{\lambda}_a} C_{ij}^{-1} \frac{\partial f_j(\lambda)}{\partial \bar{\lambda}_b} \ . \end{aligned} \tag{14}$$

These same quantities allow us to estimate the error in the λ_a. The $\bar{\lambda}_a$ are implicitly functions of the $\bar{Y}_i$, so it is meaningful to define

$$\Delta_{ab} = \langle (\bar{\lambda}_a - \bar{\bar{\lambda}}_a)(\bar{\lambda}_b - \bar{\bar{\lambda}}_b) \rangle \ , \tag{15}$$

where the average is over our assumed probability distribution for the $\bar{Y}_i$. Expanding the $\bar{\lambda}_a$ about $\bar{\bar{\lambda}}_a$ to lowest order gives

$$\bar{\lambda}_a - \bar{\bar{\lambda}}_a = \frac{\partial \bar{\lambda}_a}{\partial \bar{Y}_k}(\bar{Y}_k - \bar{\bar{Y}}_k) \tag{16}$$

giving us

$$\begin{aligned} \Delta_{ab} &= \frac{1}{Z}\int [d\bar{Y}] \exp[-\tfrac{1}{2}(\bar{Y}_i - \bar{\bar{Y}}_i)(C^{-1})_{ij}(\bar{Y}_j - \bar{\bar{Y}}_j)] \\ &\quad \times (\bar{Y}_k - \bar{\bar{Y}}_k)\frac{\partial \bar{\lambda}_a}{\partial \bar{Y}_k}\frac{\partial \bar{\lambda}_b}{\partial \bar{Y}_l}(\bar{Y}_l - \bar{\bar{Y}}_l) \\ &= \frac{\partial \bar{\lambda}_a}{\partial \bar{Y}_k} C_{kl} \frac{\partial \bar{\lambda}_b}{\partial \bar{Y}_l} \ . \end{aligned} \tag{17}$$

We can determine the $\partial \bar{\lambda}_a / \partial \bar{Y}_i$ from implicit differentiation of the minimization condition, Eq. (13), with respect to $\bar{Y}_i$:

$$\begin{aligned} 0 &= 2\frac{\partial f_i}{\partial \bar{\lambda}_a \bar{\lambda}_b}\frac{\partial \bar{\lambda}_b}{\partial \bar{Y}_i} C_{jk}^{-1}[f_k(\bar{\lambda}) - \bar{Y}_k] \\ &\quad + 2\frac{\partial f_j}{\partial \bar{\lambda}_a} C_{jk}^{-1}\frac{\partial f_k}{\partial \bar{\lambda}_b}\frac{\partial \lambda_b}{\partial \bar{Y}_i} - 2\frac{\partial f_j}{\partial \bar{\lambda}_a} C_{jk}^{-1}\delta_{ki} \ . \end{aligned} \tag{18}$$

Using the definition of the Hessian and solving for $\partial \bar{\lambda}_b / \partial \bar{Y}_i$ we get

$$\frac{\partial \bar{\lambda}_b}{\partial \bar{Y}_i} = 2H_{ba}^{-1}\frac{\partial f_j}{\partial \bar{\lambda}_a} C_{ji}^{-1} \tag{19}$$

and this gives us

$$\Delta_{ab} = 4H_{ac}^{-1}\frac{\partial f_i}{\partial \bar{\lambda}_c} C_{ij}^{-1}\frac{\partial f_j}{\partial \bar{\lambda}_d} H_{db}^{-1} \ . \tag{20}$$

Note that if the fit is a good one, $(f_j - \bar{Y}_j)$ is small and

$$\Delta_{ab} \approx 2H_{ab}^{-1} \ , \tag{21}$$

the usual approximation. Since we have all the terms available, we use the full expression in Eq. (20).

From the definition of Δ in Eq. (15), the probability distribution for finding a set of parameters $\bar{\lambda}_a$ is

$$\exp\left[-(\bar{\lambda}_a - \bar{\bar{\lambda}}_a)\frac{\Delta_{ab}^{-1}}{2}(\bar{\lambda}_b - \bar{\bar{\lambda}}_b)\right] \ . \tag{22}$$

Thus the contour lines of the quadratic form in the exponent of Eq. (22) define the allowed range of the parameters. Here we will quote one-standard-deviation errors, or the range of parameters over which

$$(\bar{\lambda}_a - \bar{\bar{\lambda}}_a)\Delta_{ab}^{-1}(\bar{\lambda}_b - \bar{\bar{\lambda}}_b) < 1 \ . \tag{23}$$

Within the accuracy of our quadratic approximation this is equivalent to asking how much the parameters can be varied without raising χ^2 by more than one unit from its minimum value. [There is an amusing analogy with the Monte Carlo renormalization group here. Consider the $\bar{Y}_i$ in Eq. (9) to be the original variables of a system with a quadratic Hamiltonian $\frac{1}{2}C^{-1}$ and the parameters $\bar{\lambda}_a$ as the variables of a "blocked" system with renormalized Hamiltonian $\frac{1}{2}\Delta^{-1}$.]

If we are interested in the allowed range, or probability distribution, of a subset of the parameters examination of Eq. (15) reveals that we should use the submatrix of Δ corresponding to the parameters of interest. For example, if we are interested in two masses, parameters 1 and 3, then we find their allowed range (the other parameters being allowed to vary freely) from the quadratic form

$$(\lambda_1 - \bar{\lambda}_1 \quad \lambda_3 - \bar{\lambda}_3)\frac{\tilde{\Delta}_{13}^{-1}}{2}\begin{bmatrix} \lambda_1 - \bar{\lambda}_1 \\ \lambda_3 - \bar{\lambda}_3 \end{bmatrix} \ , \tag{24}$$

where

$$\tilde{\Delta}_{13} = \begin{bmatrix} \Delta_{11} & \Delta_{13} \\ \Delta_{31} & \Delta_{33} \end{bmatrix} \ . \tag{25}$$

As a trivial special case, if we are interested in one pa-

rameter its statistical error is given by the square root of the corresponding diagonal element of Δ. The off-diagonal elements of Δ are the correlations among the parameters—if parameter a increases by ϵ then parameter b will increase by $\Delta_{ab}\epsilon$. Since Δ is positive definite the rescaled parameter correlations

$$\frac{\Delta_{ab}}{(\Delta_{aa}\Delta_{bb})^{1/2}} \tag{26}$$

are all less than one in magnitude. It is generally necessary to take these parameter correlations into account when computing the error on a function of several parameters. For example, the difference of two masses, parameters 1 and 2, is

$$\lambda_1-\lambda_2\pm(\Delta_{11}+\Delta_{22}-2\Delta_{12})^{1/2}\ . \tag{27}$$

Sometimes we are interested in the ratio of masses obtained in two different propagators but from the same data set, notably in computing the N/ρ mass ratio. In this case the strictly correct thing to do is to simultaneously fit the ρ and N propagators, keeping track of the correlations among all the parameters. We then include the parameter correlations in the error estimate, using

$$\frac{\lambda_1}{\lambda_2}\pm\frac{\lambda_1}{\lambda_2}\left[\frac{\Delta_{11}}{\lambda_1^2}+\frac{\Delta_{22}}{\lambda_2^2}-\frac{2\Delta_{12}}{\lambda_1\lambda_2}\right]^{1/2}, \tag{28}$$

where parameters 1 and 2 are the two masses. Notice that the values for the masses in such a combined fit will differ slightly from the masses obtained in separate fits to the nucleon and ρ propagators due to the effect of the correlations between elements of the two propagators. The nucleon to ρ mass ratios for the $aT_c=\frac{1}{6}$ runs are computed in this way. We found however, that the correlations among parameters in different propagators, such as the nucleon and ρ masses, are generally fairly small. For example, in the six runs with $aT_c=\frac{1}{6}$ the rescaled parameter correlations, Eq. (26), of the ρ and N masses in a combined fit using the distance ranges discussed in Sec. IV range from -0.174 ($am_q=0.05$, $6/g^2=5.47$, $10^3\times24$) to $+0.173$ ($am_q=0.025$, $6/g^2=5.4375$, $8^3\times24$). Of the six $aT_c=\frac{1}{6}$ runs, the largest effect is in the run with $am_q=0.025$ on the $10^3\times24$ lattice, where the combined fit produces a ratio of 1.70(19) while naively combining the results from separate fits produced 1.64(21). Given the smallness of these correlations we do not include them in other mass ratios, notably in the π to ρ mass ratios where the errors in the π mass are small enough to be negligible anyway.

With the correlations properly accounted for, χ^2 has its usual interpretation as an indicator of the goodness of the fit; i.e., we expect χ^2 to be about 1 per degree of freedom. We will generally give the goodness of fit as a "confidence level," which is the probability that a run with the errors we have estimated and a fitting function which is correct would produce a χ^2 larger than the one we find. Having a built-in indicator of the goodness of fit is as important a benefit of including the correlations as having improved parameter estimates and reliable statistical error estimates.

As an example of the effects of including the correlations among different distances consider fits to the pion propagator containing one particle—a single hyperbolic cosine— with $am_q=0.025$, $6/g^2=5.4375$ on a $10^3\times24$ lattice. If we fit to the distance range from two to the center of the lattice without considering correlations we find $m_\pi=0.4541(27)$, with $\chi^2=4.7$ for 9 degrees of freedom—apparently a very good fit. However, when we include the correlations in a fit to this same distance range we find $m_\pi=0.4577(8)$ with $\chi^2=126.2$ for 9 degrees of freedom, showing that this was really a very bad fit. For a minimum distance of seven, which we will actually use, the naive fit gives $m_\pi=0.4482(54)$ with $\chi^2=0.03$ for 4 degrees of freedom, while the correct fit is 0.4490(14) with $\chi^2=2.77$ for 4 degrees of freedom. Since the propagators at different distances have positive correlations, meaning they tend to move up or down together, the statistical errors on the masses are usually less than would be obtained in a naive fitting, as in the above example.

The quadratic approximation for χ^2 about its minimum may not be good over the one standard deviation range of the parameters, especially in cases where the fractional error is large. To explore this question we make plots of χ^2 as a function of one of the parameters, allowing the other parameters to adjust themselves to minimize χ^2. In Fig. 1 we show such a plot for a two-parameter (one-particle) fit to the pion propagator of $am_q=0.025$, $6/g^2=5.4375$ on a $10^3\times24$ lattice, using distances from 8 to 12. In this case, the quadratic approximation is good and the result given by our fitting program, 0.4480 ± 0.0017, needs no modification. In contrast, a fit to the same propagator with four parameters over distances from 4 to 12 produces the second curve in Fig. 1, where the parabola is visibly distorted. Here we should probably quote $m_\pi=0.4478^{+0.0018}_{-0.0048}$ rather than the $m_\pi=0.4478\pm0.0025$ as given by the curvature at the minimum. In most of our fits the quadratic approximation is quite good, and we generally use errors estimated

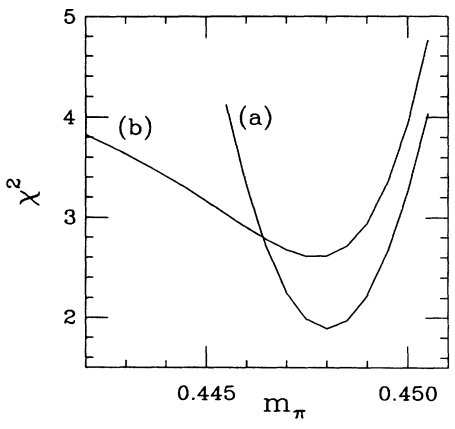

FIG. 1. χ^2 as a function of pion mass. Curve (*a*) is a one-particle fit to distances 8–12, with 3 degrees of freedom. The amplitude is allowed to vary to minimize χ^2 for each mass. Curve (*b*) is a two-particle fit to distances 4–12, with 5 degrees of freedom, with the other three parameters allowed to vary freely.

in this way. This particular problem will diminish with larger scale simulations, since as the error bars become smaller the higher derivatives of χ^2 with respect to the parameters will be less important over the range of the error bar.

III. CONTROL OF SYSTEMATIC ERRORS

We are now ready to discuss the parameters in our simulation and how we have attempted to control the systematic errors. These parameters fall into two categories: those that are present in any QCD simulation and those that are specific to a particular numerical technique. The former group consists of the quark mass, gauge coupling, spatial and temporal lattice sizes, and the number of (uncorrelated) configurations in the sample. In the latter group, we have the stopping criterion for the iterative technique used to invert the fermion matrix and the finite-step size used to integrate the molecular-dynamics equations of motion.

A. Bare couplings and lattice size

The bare-quark mass and gauge coupling are the most prominent parameters of any simulation. Among the hadrons, the pion is most sensitive to the quark bare mass because, as an approximate Goldstone boson, its mass is going to zero as the bare-quark mass goes to zero. In principle, the quark mass should be adjusted so that the mass ratio of the π and some other hadron such as the ρ has its measured value. In practice, simulations have not been done with sufficiently small quark mass to achieve this and an extrapolation is done from larger values. Our hadron masses are initially given in lattice spacing units for fixed bare coupling and quark mass.

It is well known that for a theory with a dimensionless coupling constant such as QCD, picking the coupling is equivalent to picking the lattice spacing. In QCD the physical limit (zero-lattice spacing) is the weak-coupling limit. Any convincing spectrum calculation must demonstrate appropriate scaling behavior as the lattice spacing is reduced. Pure gauge QCD spectrum calculations on large lattices are reaching this point,[8] but we make no attempt to do this here. Since the bare couplings determine the physical lattice spacing the lattice size and couplings must be discussed together. The physical limit of any lattice calculation is the infinite volume and zero-lattice-spacing limit; however, there are practical limits of available computer time which constrain any simulation. It is essential to pick a box large enough to avoid finite-size effects, but small enough that the simulation can be carried out in a reasonable length of time.

There has been some work attempting to measure the size of hadrons in a simulation.[4] This would provide a self-consistent way to demonstrate that one's spatial box is large enough if there were a known quantitative connection between the particle mass and the wave function at the edge of the box. That not being the case, we use the more straightforward technique of carrying out each simulation with two different spatial sizes and comparing the results. This will be discussed in Sec. IV.

The temporal size of the lattice must also be chosen carefully. Each hadronic source also couples to excited states. If the lattice is too short in the time direction, then even at the maximum distance from the source the propagator will not be falling exponentially with a mass characteristic of the lowest-mass particle in the given channel. In principle, we could sort this out with a many parameter fit, but in practice our fitting is much more credible if the lowest-mass particle dominates the propagator over at least part of the distance range included in the fit. The effective mass plot is a simple way of demonstrating whether a lattice is long enough in the time direction. The effective mass as a function of the distance from the source is defined by using the propagator at two distances and assuming that only a single particle is present in the channel. For mesons, the equation

$$\frac{P(t+\delta)}{P(t)}=\frac{e^{-m_t(t+\delta)}+e^{-m_t(T-t-\delta)}}{e^{-m_t t}+e^{-m_t(T-t)}} \tag{29}$$

is solved for the effective mass m_t. For the pion we may set $\delta=1$ because the opposite-parity terms in Eq. (4) are absent. For the ρ we take $\delta=2$ so that the neglected opposite-parity terms will not be alternating in sign. For the nucleon we also take $\delta=2$ and the sign in front of the second term in both the numerator and denominator of Eq. (29) changes. Before examining plots of the effective masses, we present our choices for the couplings and lattice size.

We have run our simulations with six values for the pair of bare couplings am_q and $6/g^2$. In pure gauge theory spectrum calculations a fixed coupling value is used with several quark masses. However, in a calculation with dynamical fermions, the renormalized coupling depends upon both the bare coupling and the quark mass. This being the case, we vary both $\beta=6/g^2$ and m simultaneously to try to hold a physical length scale fixed. The physical length scale comes from our study of QCD at high temperatures.[16] There is a rapid crossover for both the Polyakov loop and $\langle\bar{\psi}\psi\rangle$ as the coupling is varied, corresponding to a restoration of chiral symmetry as the temperature is raised.[17] We choose to regard the chiral-restoration temperature as the constant physical quantity. Of course, this is an approximation since the chiral-restoration temperature almost certainly depends on the quark masses.

In our earlier study, we measured $6/g^2$ at the crossover for several quark masses with four lattice spacings in the Euclidean time direction. Thus, we have measured the values of $6/g^2$ for which $aT_c=\frac{1}{4}$, where T_c is the crossover temperature. (Even for quark masses where there appears to be no real high-temperature phase transition the crossover to high-temperature behavior is sufficiently fast to define a crossover $6/g^2$.) We have also made rough measurements of the crossover values of $6/g^2$ on $10^3\times 6$ and $12^3\times 6$ lattices, or $aT_c=\frac{1}{6}$. Within the accuracy of these measurements, $6/g_c^2$ for $N_t=6$ can be found by adding 0.15 to $6/g_c^2$ for $N_t=4$. [For the pure gauge theory the difference is 0.185(25).]

For $6/g^2$ such that $aT_c=\frac{1}{4}$ we choose quark masses of 0.1, 0.05, and 0.025 on $6^3\times 24$ and $8^3\times 24$ lattices. Since $1/aT_c=4$ these lattices are clearly large enough to

prevent "deconfinement" in the spatial directions.[18] We ran two spatial sizes for each coupling to study finite-size effects. For each coupling and lattice size we ran for 1000 molecular dynamics time units, refreshing the momenta after each time unit. (We refer to the molecular-dynamics integration from one refreshing to the next as a "trajectory.") For $am_q=0.1$ and 0.05 we used a time step Δt of 0.04, so each run involved 25 000 updatings of the lattice. For $am_q=0.025$ we used $\Delta t=0.02$, so we have 50 000 steps in each run. Before each run we made 100 warm-up trajectories of one time unit each. For $am_q=0.1$ we began with an ordered lattice and for other quark masses we began with an equilibrated lattice at the next-higher quark mass. On the $8^3\times 24$ lattices we measured propagators every two time units, giving 500 propagators, while for the $6^3\times 24$ runs we made fewer measurements. In each propagator computation we used only a single source point, but computed three propagators—one for a source of each color.

For $aT_c=\frac{1}{6}$ we also ran at $am_q=0.1$, 0.05, and 0.025 but using lattice sizes of $8^3\times 24$ and $10^3\times 24$. Again, in each case we ran 1000 time units. In all these runs we measured a propagator every two time units.

We also ran quenched simulations on $10^3\times 24$ lattices for $am_q=0.05$ and 0.025 at $6/g^2=5.865$, the pure gauge deconfinement coupling for $N_t=6$. This is analogous to our weaker coupling for the full QCD simulations. However, it is not necessarily true that the pure gauge deconfinement temperature is the same as the full QCD chiral-restoration temperature.[19] Indeed, the only case in which it makes sense to quote results in MeV is full QCD with the correct quark masses. As we shall see in Sec. V, if the pure gauge theory deconfinement temperature and full QCD chiral-restoration temperature are assumed to be the same, meaning that our physical lattice spacing is the same in our quenched and weaker coupling full QCD simulations, the pure gauge QCD hadrons are lighter than the full QCD hadrons. Conversely, if the ρ or nucleon masses are taken to be the same in pure gauge QCD as in full QCD, the transition temperature is higher in pure gauge QCD than in full QCD. Table II summarizes the parameters of the various runs.

The data sets we present in greatest detail are the ones corresponding to the $10^3\times 24$ lattice with the weaker couplings (corresponding to $aT_c=\frac{1}{6}$) and masses of $am_q=0.10$ and 0.025. These data sets are most interesting because they are closest to the continuum limit. The heavier mass indicates how well one can do while the lighter one shows how difficult it can be to fit the propagators. For comparison we will also show graphs from the quenched calculation with $am_q=0.025$.

With these details in mind we are ready to show effective mass plots for the π, ρ, and nucleon at the two mass values. In Figs. 2(a) and 2(b) we show the effective π mass. for $am_q=0.10$ we see a flat region starting at distance 6 and continuing to 11. For $am_q=0.025$, the flat region begins at distance 5 or 6 and continues all the way across the lattice. In Figs. 3(a) and 3(b) we see that the situation for the ρ is not nearly so nice. With $am_q=0.10$ we find a fairly flat region from 4 to 9. However, for $am_q=0.025$, there are such large statistical errors on the ρ propagator that we cannot plot points at a distance greater than 8, and it is clear that there is no region we could call a plateau. Let us emphasize that with the number of samples we have we cannot measure the ρ propagator accurately halfway across this lattice, so there is nothing to indicate that a longer lattice would be an improvement.

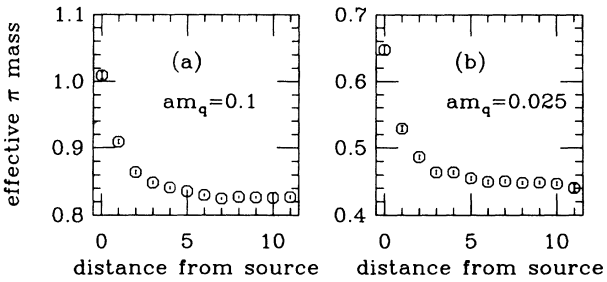

FIG. 2. Effective pion mass as a function of distance from the source. We show results for (a) $am_q=0.1$, $6/g^2=5.525$ and (b) $am_q=0.025$, $6/g^2=5.4375$ on the $10^3\times 24$ lattice.

The effective mass plot for the nucleon shown in Fig. 4 shows an interesting pattern. Recall that for the nucleon we also use $\delta=2$. Therefore, each value plotted depends on only even or only odd distances. We see that for $am_q=0.10$ the even distance values are very stable. The odd distance values are larger and fall smoothly to meet the even distance values almost half-way across the lattice. This behavior can be interpreted as destructive interference of the N^* and $\tilde{N}$ on the even sites. For $am_q=0.025$, the nucleon propagator is negative at distance 10 and 11 so we cannot plot points at distance 8 or greater; however, a pattern similar to that at $am_q=0.10$ is observed.

B. Number of independent configurations

Now we return to the issue of the number of independent configurations in the simulation. In order to investigate this issue we plot time histories of propagator elements and effective masses, and we also calculate autocorrelation functions. The time histories allow us to judge whether there are long time fluctuations in the propagators.

In Fig. 5 we show the time history of the π propagator

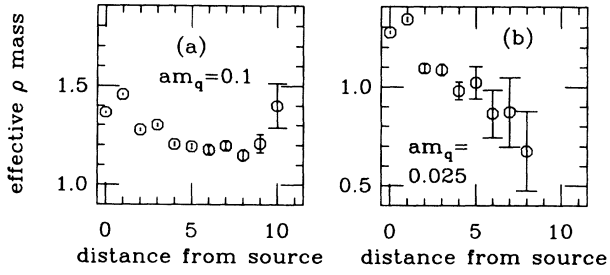

FIG. 3. Effective ρ mass vs distance from the source. We show results from the same runs as Fig. 2.

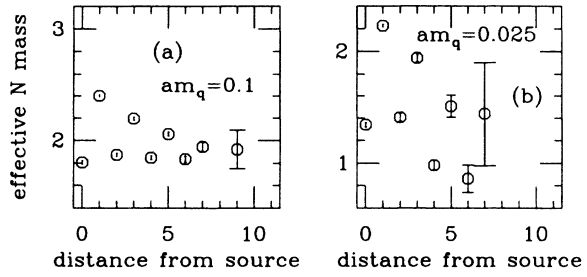

FIG. 4. Effective nucleon mass vs distance from the source for the same two runs as Fig. 2.

at distances 4 and 8 from the source for $am_q=0.025$ on the $10^3\times 24$ lattice. We note that there are some large non-Gaussian fluctuations, and that there are short time correlations on the order of several trajectories. If there are long time correlations, they apparently are on a scale much longer than 1000 trajectories. In Fig. 6(a) we show the autocorrelation of the π propagator at distance 4 from the source. The plotting symbol is about as large as the error would be if the data were uncorrelated. We remind the reader that in these runs we averaged ten successive π propagators before beginning the analysis of Sec. II.

In Fig. 7 we show the time history of the ρ propagator at distances 4 and 8 for the same run, and in Fig. 8 the nucleon propagator. (Note that the nucleon propagator at even distances is small because of cancellation between baryons of opposite parity, so the spikes are exaggerated here.) The autocorrelation of the ρ and nucleon propagators are almost always less than 0.15 at all nonzero times and all distances. Most of the exceptions are at short distances from the source.

We are interested in the propagator elements as a means to calculate the mass of the hadrons, and it is possible that correlations are more easily seen in the masses

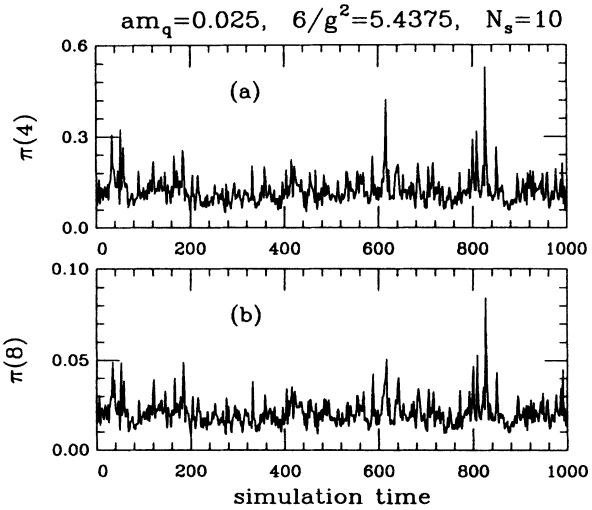

FIG. 5. Simulation time histories of pion propagator. We plot the sum of the propagator over a spatial slice at a given distance in Euclidean time from the source point. These plots are for $am_q=0.025$ and distances (a) 4 and (b) 8.

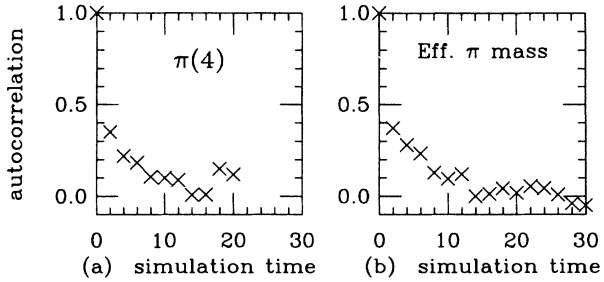

FIG. 6. Autocorrelation of the pion propagator at distance (a) 4 and for the pion effective mass from distances (b) 7–9 for $am_q=0.025$ and $6/g^2=5.4375$ on the $10^3\times 24$ lattice. The symbol size is the statistical error for the autocorrelation on an uncorrelated sequence of this length.

than in the raw propagator elements. We may use the effective mass to calculate a particle mass from the propagator on a single configuration. It is interesting to plot a time history of the effective mass. In Fig. 9 we use Eq. (20) with $\delta=2$ and plot the effective mass using the π propagator at distances 7 and 9 from the source. This is the distance range that is most important in our determination of the mass in Sec. IV. The fluctuations in effective mass grow as we move farther from the source. Figure 6(b) shows the autocorrelation of this effective mass for this run. The autocorrelation of the effective mass is larger than the autocorrelation of the propagator itself at this distance—at a distance from the source of eight lattice spacings the autocorrelation of pion-propagator measurements separated by two simulation time units is unmeasurable. The fluctuations of the ρ propagator are much larger than for the π and the effective mass time history can only be plotted for short distances from the source, since for large distances the propagators do not consistently decrease in size as the distance increases. It is possible to block a certain number of propagators together, which improves the situation, but not sufficiently to warrant including a plot.

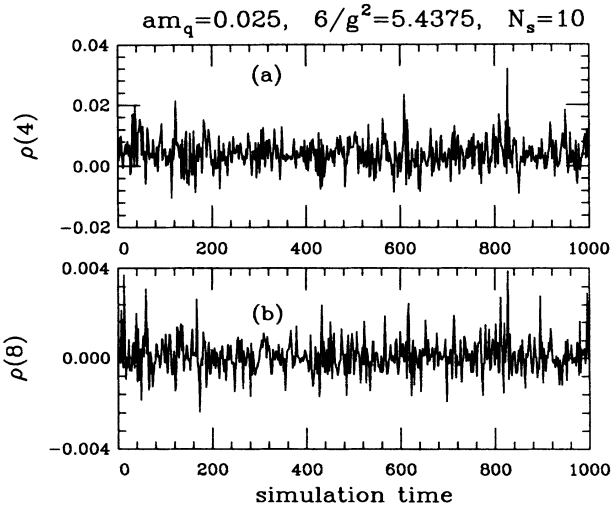

FIG. 7. Time history of the ρ propagator for distances (a) 4 and (b) 8 with $am_q=0.025$.

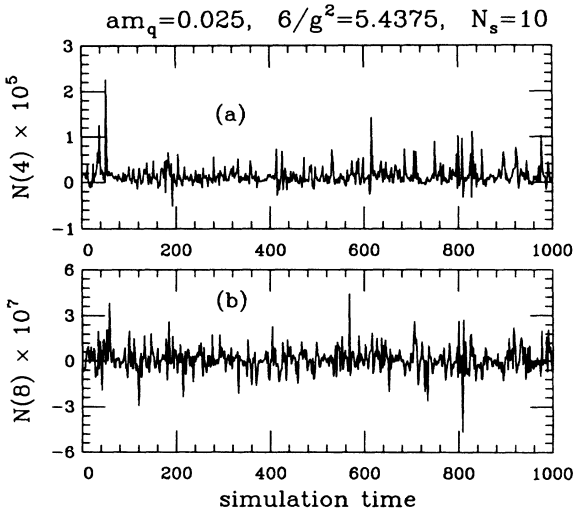

FIG. 8. Time history of the nucleon propagator for distances (a) 4 and (b) 8 with $am_q = 0.025$.

Yet another way to analyze the autocorrelation is to Fourier transform the time history, or compute the power spectrum. In Fig. 10 we show the square root of the power spectrum for the π effective mass for $am_q = 0.1$ and 0.025, using distances 7 and 8. The horizontal line on each graph shows the median value of this quantity for a Gaussian random variable (no autocorrelation) which would give the same statistical error on the effective mass as we obtain from blocking the time history into blocks of 20 measurements. The suppression of the power spectrum below this line at high frequencies reflects the autocorrelation in the data. Note that the frequency above which fluctuations are suppressed is about the same for both masses ($\omega \approx 0.3$) but the low-frequency noise is larger for the smaller quark mass. Again, in our analysis we average the propagators from five or ten successive measurements, or ten or twenty simulation time units, before beginning our fitting so that we are working with approximately independent measurements.

Low-mass quenched calculations with Wilson fermions have exhibited a phenomenon called "exceptional configurations."[20] In these configurations the π propagator is exceptionally large, and other propagators are often large as well. This is reminiscent of the spikes seen in the

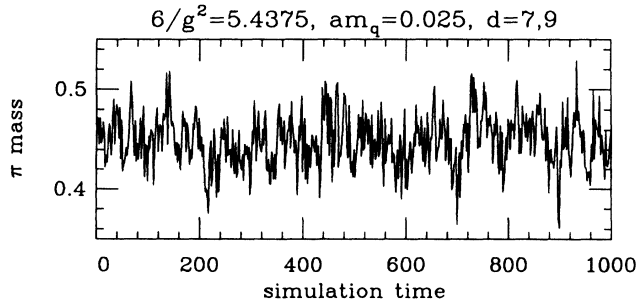

FIG. 9. Simulation time history of the pion effective mass using distances 7–9. We show results for $am_q = 0.025$ and $6/g^2 = 5.4375$.

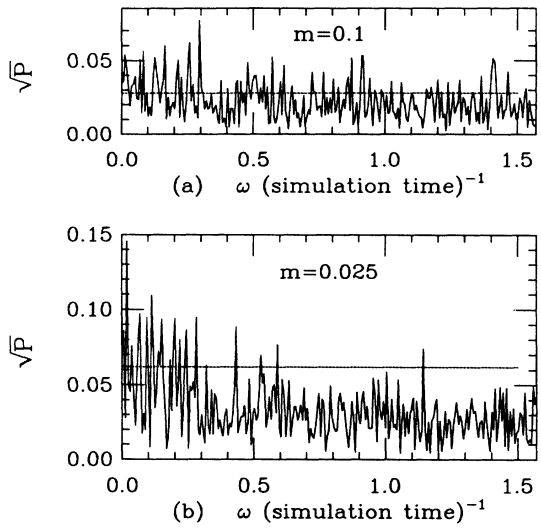

FIG. 10. The power spectrum of the pion effective mass between distances 7 and 8 on the $10^3 \times 24$ lattices for (a) $am_q = 0.1$ and (b) 0.025. The large spike at $\omega = 0$ is suppressed, and the renormalization is chosen to be independent of the run length. The horizontal lines are the median value of a white-noise power spectrum which would give the same statistical error for the effective mass as is obtained from blocking the measurements into blocks of 20. The highest frequency is $\pi/2$ since we measured every two simulation time units, and negative frequencies are not shown since they are the same as the positive frequencies.

time histories of our propagators, such as those in Figs. 5, 7, and 8. In Fig. 11(a) we show a histogram of the π propagator at a distance 10 from the source for our lightest mass and largest lattice. We see that this distribution is non-Gaussian, as was apparent from Fig. 5. Since the π propagator is the sum over all spatial sites of the absolute square of the quark propagator, it is not surprising that its distribution is not Gaussian. We see that the distribution has its peak in the bin which ends at 0.009, and that there are 13 of 500 configurations between 2 and 3 times the peak value and 1 configuration above 3 times the peak value.

This is to be compared with the quenched Wilson fermion simulation[20] in which there were 28 configurations

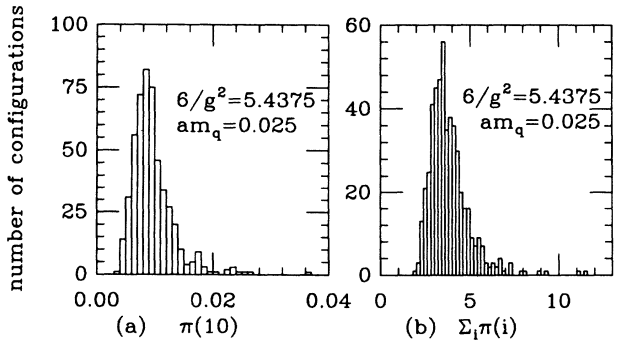

FIG. 11. Histogram of the pion propagator summed over the spatial slice at distance (a) 10 and (b) summed over distances. Again, we show results for $am_q = 0.025$ and $6/g^2 = 5.4375$.

with three source points, and forward and backward propagation were both included. In that case, 9 of 148 propagators were between 2 and 4 times the peak value and 7 were above 4 times the peak value. From this point of view, there appears to be a difference between our calculation and the quenched Wilson case.

A second way of searching for exceptional configurations is based upon summing the π propagator over all distances from the source.[20] A histogram of this quantity is shown in Fig. 11(b). We see that the distribution peaks around 3.6, but we probably would not consider configurations unusual until they exceed at least twice that value. Nine of 500 configurations exceed 7.2 and two of them are greater than 10.8. From this perspective, exceptional configurations are not all that less frequent in the present case than in the quenched calculation where 1 of 28 configurations exceeded twice the peak value. There, two configurations were between 1.5 and 2 times the peak value and a third configuration was at 3.6 times the peak value.

In summary, in this respect we do not see a dramatic difference between this dynamical Kogut-Susskind fermion calculation and the quenched Wilson case. However, a systematic exploration would really require a careful study as a function of quark mass and greater statistics since we are interested in the tail of a rapidly falling distribution. Certainly the question of whether there is a disease of either the quenched approximation or Wilson fermion formulation which is cured by using either dynamical or Kogut-Susskind fermions is an interesting one which deserves further study.

C. Conjugate-gradient residual

Because we use an iterative technique to calculate the quark propagator, we must adopt a stopping criterion and (hopefully) show that it is sufficiently stringent that our results are insensitive to it. There are two distinct uses of the fermion inversion program. During the molecular-dynamics updating, we use the program with a pseudofermion field as a source. This source is a Gaussian random vector with norm proportional to the volume. To measure the hadron propagators, we use the inversion program with a source which is a δ function in space and color. If R is the residual vector, we use $(R^2/V)^{1/2}<0.005$ during the updatings and $(R^2)^{1/2}<5\times10^{-5}$ for hadron propagators. In a previous paper,[21] we investigated the dependence of the average plaquette and $\langle\bar{\psi}\psi\rangle$ on $(R^2/V)^{1/2}$. We found that for $am_q=0.10$ or 0.05 and similar values of $6/g^2$ these quantities would not change at smaller values of $(R^2/V)^{1/2}$. For $am_q=0.025$ the plaquette was insensitive to the residual, but perceptible effects remained in $\langle\bar{\psi}\psi\rangle$. We refer the reader to Ref. 21, Figs. 7 and 8 for additional details. Since then we have done another check on $8^3\times4$ lattices in which we reduced the residual from the value 0.005 used here to 0.001. Table III shows the plaquette and $\langle\bar{\psi}\psi\rangle$ in these runs. Notice that for this lattice size the higher value of $6/g^2$ in this table, 5.32, is in the chiral-symmetric phase, where the fermion matrix is generally better conditioned. We also studied in Ref. 21 the effect of the stopping criterion on the propagator measurements and on the fitted masses. For $am_q=0.025$ and $6/g^2=5.2875$ on the $8^3\times24$ lattice we made part of the run with 200 conjugate-gradient iterations in the propagator measurements, which corresponds to a residual of about 2×10^{-3}, instead of the roughly 340 iterations required to obtain the residual of 5×10^{-5}. We found that the π propagator differed by only about 0.1% in the two parts of the run. Fitting for the π and ρ masses in the two parts of the run we found that any systematic effect on the π mass was comparable to the statistical error and any effect on the ρ much smaller than the statistical error. Thus, although we have not repeated our entire calculation with a different value for the stopping criterion, we feel confident from these studies that no significant error is introduced by our choice of residual for the propagator measurements.

D. Molecular-dynamics step size

The algorithm we use is known to have a systematic bias for finite step size which grows as $(\Delta t)^2$. We again refer the reader to our earlier work which studied the dependence of the average plaquette and $\langle\bar{\psi}\psi\rangle$ upon the step size in the high-temperature phase.[21] For slightly smaller values of $6/g^2$, $am_q=0.025$, and step size 0.02, the same as used here, we found a systematic effect on the plaquette of order 0.01, with smaller effects for the higher quark masses. (We normalize the plaquette to 3.0 at $g^2=0$.) Also, Table III contains results for the plaquette with $am_q=0.025$ with $\Delta t=0.0125$ as well as the 0.02 used here. We have not directly studied the finite step size effects upon the mass measurements.

IV. RESULTS OF FITTING THE PROPAGATORS

Having defined the propagators and fitting procedure, we now discuss the results. With our boundary conditions, meson propagators are symmetric in Euclidean time on the average. Baryon propagators are antisymmetric in time for even or odd distances, respectively, ex-

TABLE III. Effect of the molecular-dynamics step size and conjugate-gradient accuracy on local quantities. These results are from an $8^3\times4$ lattice with $am_q=0.025$.

$6/g^2$	Quantity	$\Delta t=0.02$, $(R^2/V)^{1/2}=0.005$	$\Delta t=0.0125$	$(R^2/V)^{1/2}=0.001$
5.26	Plaq.	1.446(2)	1.454(2)	1.445(2)
	$\langle\bar{\psi}\psi\rangle$	0.383(4)	0.379(3)	0.395(5)
5.32	Plaq.	1.573(2)	1.570(2)	1.575(2)
	$\langle\bar{\psi}\psi\rangle$	0.125(4)	0.129(3)	0.120(5)

cept for distance zero. This symmetry allows us to restrict our meson (baryon) propagators to the distance range 0–12 (0–11) by averaging the values at distance t and $T-t$ with the appropriate sign. The lightest particle in each channel determines the large distance falloff of the propagator. At short distances heavier particles make a significant contribution. We attempt to fit the propagators over the distance range $D_{\min}-12$ (or 11, for baryons) with up to four particles contributing. We would like to see that our mass estimates eventually become independent of $D_{\min}$ as we increase it and the short-distance heavy-particle contributions are eliminated. Our minimization program based on Newton's method does not always converge. [The most common way in which the fit fails to converge is for one mass to become very large. The large mass term is essentially a δ function at the shortest distance used in the fit. Thus, the mass-amplitude pair (two parameters) act to eliminate the shortest-distance point from the fit, and the two parameters are in fact indeterminate. Of course, such a fit is exactly the same as increasing $D_{\min}$ by one and using one fewer particle in the fitting function.] However, for each propagator in each run we generally have a large number of fits with various values of $D_{\min}$ and varying numbers of particles.

After some experimenting we found a graphical presentation of the results to be useful. For all our runs we made graphs showing the various fits as a function of $D_{\min}$. We will present these graphs for only three runs: quark mass $am_q=0.10$ and 0.025 with $aT_c=\frac{1}{6}$, and the quenched calculation with $am_q=0.025$ and $aT_c=\frac{1}{6}$, all on $10^3\times 24$ lattices. In all of these plots squares denote one-particle fits, crosses two-particle fits, and octagons and diamonds three- and four-particle fits, respectively. The parities of the particles included depend on the propagator. For the (PS) pion the second particle is an excited state with the same parity. In this channel there is no need for an opposite-parity particle. In all other cases, two-particle fits include one particle with each parity. Except for the π_2 (S) propagator, three-particle fits include two particles with the parity of the lowest-mass particle (not alternating in time), and one particle of opposite parity (alternating). In the case of the π_2 propagator, the second and third particles are σ and σ^*, both alternating in time. In those cases where we have four-particle fits they include two particles of each parity. The one-particle nucleon fits include only even-distance points or only odd-distance points.[22] Squares are used for both even- and odd-distance fits, since they can be distinguished by the value of $D_{\min}$. The quark mass is indicated on each graph, where m_V ("valence" quark) indicates the quenched calculation. In these graphs we have marked the fits with reasonable confidence levels by arrows. Except where otherwise noted, the arrows mark fits with confidence level greater than 10%. (Of course, many of these fits are much better than 10% confidence.) In some cases none of the fits were this good, so we have used a lower threshold. (This is not surprising. We have done fits for a total of 104 different averaged propagators. The confidence levels of all the fits to a propagator are very highly correlated, so even if we had a perfect fitting function we might expect about ten cases with all fits worse than 10% confidence level.) To aid comparisons among different graphs, we use the same vertical scales for all graphs for a given particle, and whenever reasonable use the same scales for different particles. In particular, all the graphs for the a_1, b_1, nucleon, opposite-parity nucleon, and excited pion use the same vertical scale. All graphs for the π_2, the σ, the ρ, and the ρ_2 use a scale twice as large. Finally, all the π graphs use a scale about 50 times as large.

We select one of the fits in order to report a mass and error for each particle. For a given channel we select a specific value of $D_{\min}$ and the number of particles in the fit which we will use for the three mass values and both lattice sizes. (We treat the data sets for $aT_c=\frac{1}{4}$ and $aT_c=\frac{1}{6}$ separately.) To choose $D_{\min}$ and the number of particles we examine the graphs of all the fits as well as the table of results of all the fits, which contains additional information such as the exact confidence levels of all the fits and the amplitudes associated with the masses. We look for two things in selecting the fit. First, the fits should have good confidence levels. To make this quantitative we compute a combined confidence level, which is the probability that the sum of the χ^2's in the set of fits would exceed the value in our runs. For a given number of particles in the fit we try to find a value of $D_{\min}$ for which the six fits have a good combined confidence level. Second, in choosing among the fits with different numbers of particles we pick the fit which gives smallest error bars, if the fits are of comparable quality. Reporting the value and accompanying error from a single fit produces an error estimate that is statistical only—it is an estimate of how much the parameters in this particular fit would vary if we repeated our run. (All the fits to a run are strongly correlated, so it would be misleading to attempt to average different fits.) It is more difficult to estimate the systematic error resulting from remaining contributions of excited states. We have not developed a quantitative way of estimating this systematic effect, but inspection of graphs such as Figs. 12–21 below can give some idea of the possible error.

In Figs. 12(a)–12(c) we show the π mass as a function of $D_{\min}$ for $am_q=0.10$ and 0.025 on a $10^3\times 24$ lattice, as well as the quenched result for $am_q=0.025$. For the six runs with dynamical quarks at $aT_c=\frac{1}{6}$, including the runs displayed in Figs. 12(a) and 12(b), we find that the masses determined in the single-particle fits decrease as $D_{\min}$ is increased for small $D_{\min}$, but that by $D_{\min}=6$ we are in the asymptotic region. The arrows on the figure point to masses for which the fit gives a confidence level greater than 10%. We see that to get such a fit we must have $D_{\min}=6$ for $am_q=0.10$ or $D_{\min}=5$ for $am_q=0.025$. Looking at the effective mass plots in Fig. 2 these values of $D_{\min}$ seem reasonable. We find that if we try two-particle fits we have reasonable fits in the region $D_{\min}=2-4$. These fits agree with the good single-particle fits, but their errors are larger. Table IV shows the combined confidence levels of the one- and two-particle pion fits. We choose the single-particle fits with $D_{\min}=7$,

which are shown in Table V. From similar considerations, we also use single-particle fits with $D_{\min}=7$ for the $aT_c=\frac{1}{4}$ and for the quenched data. We will discuss the dependence of the pion mass on the quark mass later.

In Fig. 13 we show our results for fitting the ρ propagator. The $aT_c=\frac{1}{6}$ ρ is much harder to fit than the π. We find few fits to individual runs with confidence level greater than 0.50. Indeed for $am_q=0.1$ on the $10^3\times 24$ lattice we found only one fit with confidence level greater than 0.1, so we have marked fits with confidence level greater than 0.05 in Fig. 13(a). Focusing on the single-particle fits first, we see that the masses bounce up and down with $D_{\min}$ odd tending to be high. This oscillatory behavior occurs because there is a significant opposite-parity contribution at short distances. Looking at the two-particle fits we see that the ρ mass drops as $D_{\min}$ increases and the tendency to bounce up and down is no longer apparent. This monotonic change in the mass as $D_{\min}$ increases is due to the contribution to the propagator of heavier states with the same parity as the ρ. With three-particle fits, the mass does not vary much with $D_{\min}$. For the $aT_c=\frac{1}{6}$ runs, the single-particle fits with $D_{\min}=7$, with a combined confidence level of 0.004, are comparable to the two-particle fits with $D_{\min}=4$, which have a combined confidence level of 0.006. For $D_{\min}=8$ the single-particle fits have a combined confidence level of 0.002, no better than for $D_{\min}=7$. We choose the $D_{\min}=7$ single-particle fits because examining the complete set of graphs such as Fig. 13 and the corresponding tables suggests that the two-particle fits have not necessarily leveled out at $D_{\min}=4$. The three-particle fits have slightly better confidence levels, but there are few enough values of $D_{\min}$ available for them that we are less certain of their convergence. For the quenched runs, the single-particle fits with $D_{\min}=7$ still have very poor confidence levels, but for $D_{\min}=8$ the fits are good (a combined confidence level for the two fits of 0.61) so we use $D_{\min}=8$. For the $aT_c=\frac{1}{4}$ data, the fits are better and we report ρ masses from the two-particle $D_{\min}=2$ fits, with a

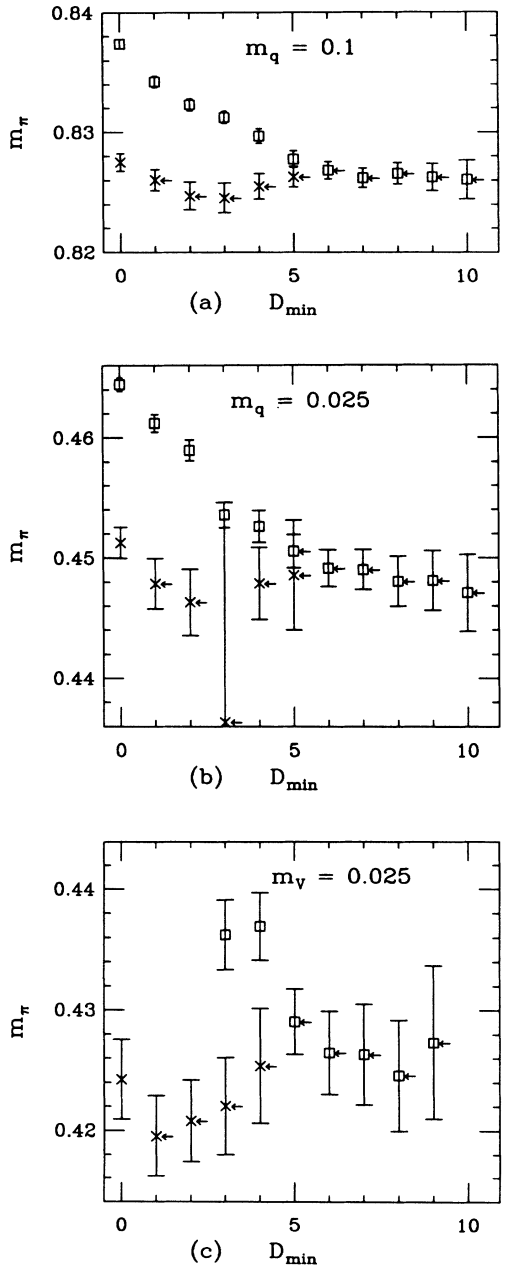

FIG. 12. Fits to the π mass on $10^3\times 24$ lattices. We show fits for (a) $am_q=0.1$, $6/g^2=5.525$, (b) $am_q=0.025$, $6/g^2=5.4375$, and (c) a quenched calculation with $am_q=0.025$ and $6/g^2=5.865$. The meaning of the symbols is described in the text.

TABLE IV. Combined confidence levels for different pion fits. The first column is the number of particles in the fit, and the second is the minimum distance included in the fit. We give the total χ^2 and number of degrees of freedom (DF) for the six runs at $aT_c=\frac{1}{4}$ and the six runs at $aT_c=\frac{1}{6}$, as well as the combined confidence level (C.L.). For the $aT_c=\frac{1}{6}$ runs, 10 measurements over 20 time units were blocked together before fitting, while for the $aT_c=\frac{1}{4}$ runs, five measurements were blocked.

Particles	$D_{\min}$	$\sum\chi^2$	DF	CL
		$aT_c=\frac{1}{4}$		
1	4	73.5	42	0.001
1	5	63.4	36	0.003
1	6	53.1	30	0.004
1	7	27.9	24	0.27
1	8	21.5	18	0.26
		$aT_c=\frac{1}{6}$		
1	4	167	42	3×10^{-20}
1	5	74.0	36	9×10^{-5}
1	6	39.6	30	0.11
1	7	24.2	24	0.46
1	8	16.6	18	0.56
1	9	9.7	12	0.66
2	0	129	54	5×10^{-9}
2	1	73.3	48	0.01
2	2	48.9	42	0.23
2	3	40.3	36	0.29
2	4	36.0	30	0.21
2	5	27.3	24	0.30

TABLE V. Pion mass estimates and their confidence levels. In all cases we use single-particle fits with $D_{\min}=7$. The V ("valence") tag on the quark mass indicates a quenched calculation. No entry indicates that we did not measure this operator during the indicated run or that there was no such run. The "small" and "large" columns refer to the smaller and larger lattice at each coupling—$6^3\times 24$ and $8^3\times 24$ for the $aT_c=\frac{1}{4}$ runs and $8^3\times 24$ and $10^3\times 24$ for the $aT_c=\frac{1}{6}$ runs. The quoted errors are statistical only.

am_q	$6/g^2$	Small	C.L.	Large	C.L.
0.1	5.375	0.8120(19)	0.59	0.8088(7)	0.23
0.05	5.32	0.5833(17)	0.67	0.5827(7)	0.05
0.025	5.2875	0.4213(20)	0.14	0.4184(9)	0.93
0.1	5.525	0.8315(10)	0.61	0.8262(8)	0.82
0.05	5.47	0.6123(17)	0.75	0.6099(10)	0.36
0.025	5.4375	0.4496(20)	0.02	0.4490(17)	0.75
0.05(V)	5.865			0.5877(27)	0.0002
0.025(V)	5.865			0.4263(42)	0.84

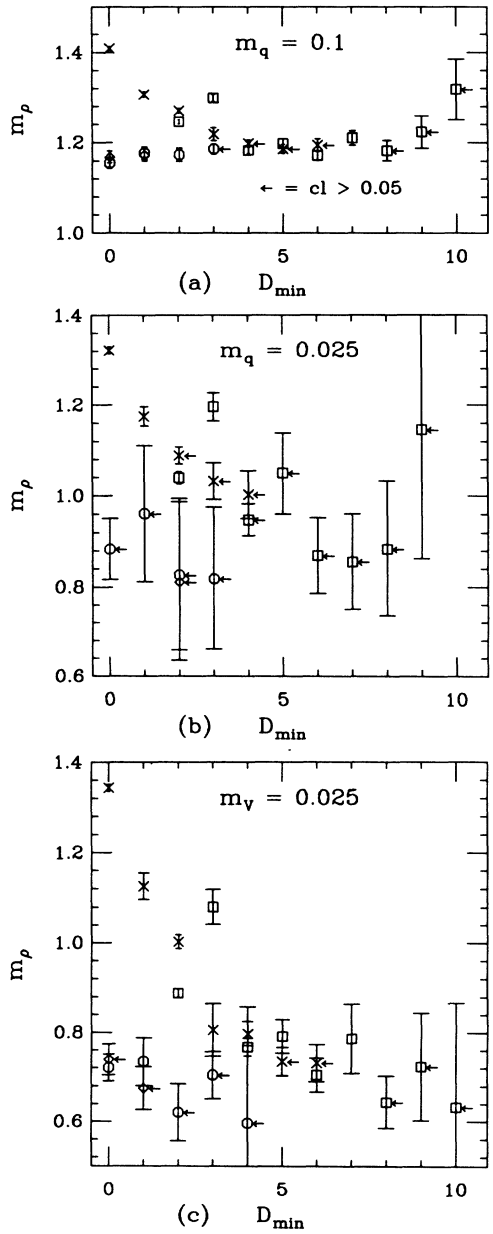

FIG. 13. Fits to the ρ mass on $10^3\times 24$ lattices for the same runs as Fig. 12.

combined confidence level of 0.41. These ρ mass estimates are in Table VI. We know of no good reason for the ρ (VT) propagator to be harder to fit than the PV or S propagators.

For most of the $aT_c=\frac{1}{6}$ runs we measure propagators for additional mesons. The Kogut-Susskind fermion formalism breaks the SU(4)×SU(4) symmetry of the four-flavor continuum theory with terms proportional to the lattice spacing a. The lowest states in the S and PV channels, the π_2 and ρ_2 should be degenerate with the π and ρ, respectively, in the limit $a\to 0$. In Fig. 14 we show our fits for the π_2 mass. The fits are quite good and we tabulate the results for the three-particle $D_{\min}=0$ fits, which have a combined confidence level of 0.80 (0.73 for the two quenched runs), in Table VII. It is immediately apparent that the π_2 is considerably heavier than the π, so there is substantial flavor-symmetry breaking. Note that this is much better in the $aT_c=\frac{1}{6}$ quenched calculation, where it is already apparent that the π_2 is becoming a low-mass particle.

In Fig. 15 we plot our mass fits for the ρ_2. Again the fits are good, and we choose the two-particle $D_{\min}=4$ fits, which have a combined confidence level of 0.72 for the six $aT_c=\frac{1}{6}$ full QCD runs. These fits are in Table VIII. We find that the ρ and ρ_2 masses are in rough agreement. Although the two do not always agree within errors, neither one is consistently heavier.

In the S channel, the σ meson appears as the opposite-parity partner of the π. Most of our two- or three-particle fits are good. We show the masses as a function of $D_{\min}$ in Fig. 16 and tabulate the results of the three-particle $D_{\min}=0$ fits in Table IX. Since this is the same fit to the same channel that we selected for the π_2, the combined confidence levels are the same—0.80 for the six full QCD runs and 0.73 for the two quenched runs.

The a_1 is the opposite-parity partner of the ρ_2 in the PV channel, and its fits are in Fig. 17. Looking at the plot in Fig. 17(b) it at first appears that nothing can be said because the $D_{\min}=4$ two- and four-particle fits have a very small mass. However, in the four-particle fits for $am_q=0.025$, the amplitudes that go with the low masses plotted in Fig. 17(b) are consistent with zero and the higher a_1 masses are comparable to the a_1 masses ob-

TABLE VI. ρ mass estimates and their confidence levels. For the $aT_c = \frac{1}{4}$ runs we use two-particle fits with $D_{\min} = 2$ and for the full QCD $aT_c = \frac{1}{6}$ runs we use one-particle fits with $D_{\min} = 7$. For the quenched runs we use one-particle fits with $D_{\min} = 8$. The notation is the same as Table V.

am_q	$6/g^2$	Small	C.L.	Large	C.L.
0.1	5.375	1.451(19)	0.09	1.408(11)	0.55
0.05	5.32	1.315(45)	0.55	1.406(48)	0.58
0.025	5.2875	1.398(160)	0.56	1.342(46)	0.33
0.1	5.525	1.231(22)	0.01	1.210(16)	0.04
0.05	5.47	1.130(112)	0.94	0.937(45)	0.03
0.025	5.4375	0.918(286)	0.11	0.856(106)	0.25
$0.05V$	5.865			0.777(26)	0.52
$0.025V$	5.865			0.644(59)	0.56

tained from three-particle fits with the same value of $D_{\min}$. Because of this we conclude that these fits with very low mass are spurious. The a_1 masses appearing in Table X come from three-particle fits with $D_{\min} = 1$ for the full QCD runs (combined confidence level 0.75) and $D_{\min} = 3$ for the quenched runs (combined confidence level 0.26).

The b_1 is the opposite-parity partner of the ρ in the VT channel. Our attempt to determine the b_1 meson mass is not very successful. The masses displayed in Fig. 18 do not allow us to choose an appropriate value for $D_{\min}$ or the number of particles and no fits are tabulated. However the plot of the quenched data [Fig. 18(c)] is better than that for full QCD.

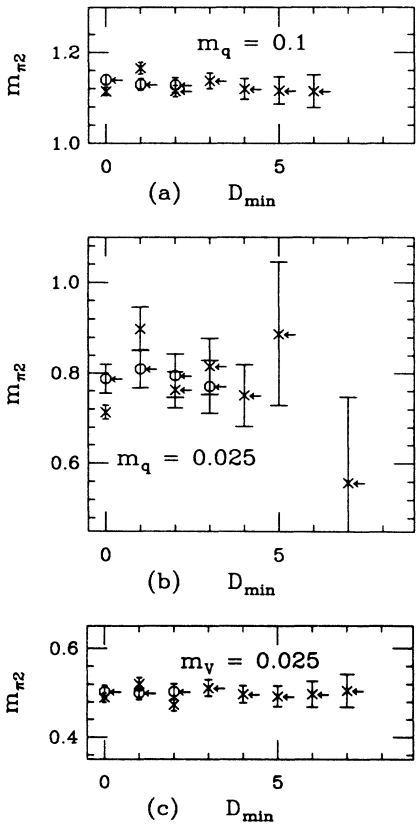

FIG. 14. Fits to the π_2 mass for the same runs as Fig. 12.

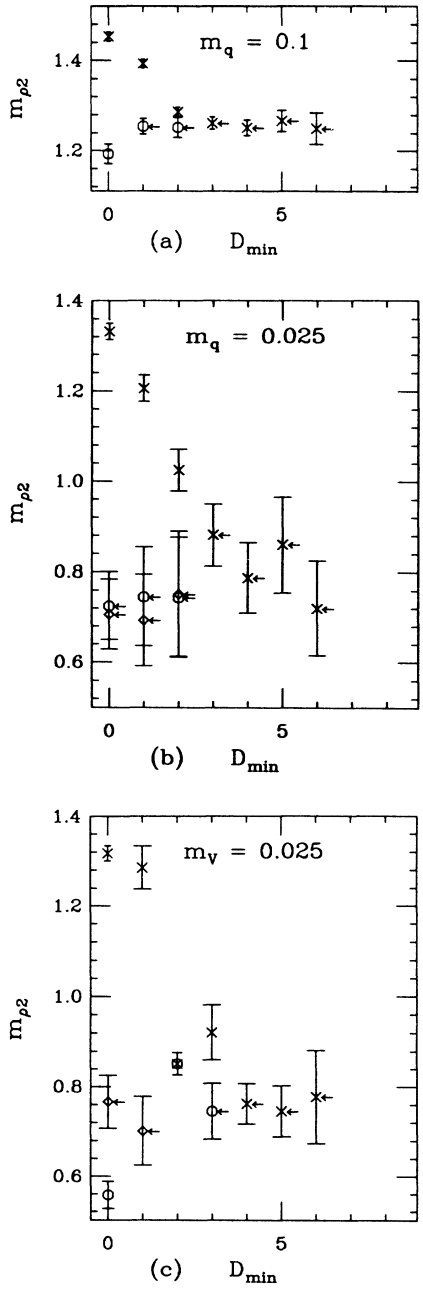

FIG. 15. Fits to the ρ_2 mass for the same runs as Fig. 12.

TABLE VII. π_2 mass estimates and their confidence levels. We use three-particle fits with $D_{\min}=0$, where both of the other particles have opposite parity (σ's). The notation is the same as Table V.

am_q	$6/g^2$	Small	C.L.	Large	C.L.
0.1	5.525			1.139(11)	0.88
0.05	5.47	0.904(43)	0.08	0.940(19)	0.85
0.025	5.4375	0.941(89)	0.75	0.788(33)	0.72
0.05(V)	5.865			0.681(11)	0.64
0.025(V)	5.865			0.503(15)	0.63

In fitting the nucleon propagator we use single-particle fits to either the even or odd distances as well as multiple-particle fits to the entire propagator. In Figs. 19(a)–19(c) we see that the fits to odd sites have the nucleon mass dropping steeply as $D_{\min}$ is increased. However, for the even sites, the nucleon mass is quite stable. In the two-particle fits we again see the mass dropping and bouncing as $D_{\min}$ is increased. This is especially pronounced for $am_q=0.10$. We see that the three-particle fits remove most of the short-distance contribution, but there is still an even-odd alternation of the mass. For the $aT_c=\frac{1}{6}$ full QCD data set we report masses from the single-particle even-sites-only $D_{\min}=4$ fits, with a combined confidence level of 0.13. The fact that the even-only fits are so stable can be interpreted as a cancellation of the effects of the N^* and $\tilde{N}$ on the even sites. This cancellation depends upon their masses and amplitudes. In the $aT_c=\frac{1}{4}$ data set we see no such effect. There we report masses from the two-particle $D_{\min}=4$ fits, with a combined confidence level of 0.34. For the quenched runs, the even distance only fits with $D_{\min}=6$ had much better confidence levels than $D_{\min}=4$ (0.59 vs 0.05), so we use $D_{\min}=6$. These masses are in Table XI. For the opposite-parity nucleon, including the fits in Fig. 20, we do not quote a mass since it is not clear that the fits have converged with respect to $D_{\min}$.

For the excited states our mass results are generally poor. The corrections to the asymptotic form (one particle with each set of quantum numbers) of the propagators can generally be well described by exponentials, as evidenced by the fact that the fits with small $D_{\min}$ containing excited states generally give the same results for the ground-state masses as do one- or two-particle fits with large $D_{\min}$, as illustrated in Fig. 12. In general, it is not clear if we are seeing an excited state, a fit to a large number of excited states, a single particle plus a pion, or lattice artifacts—things that would not scale in the continuum limit. Since the pion (PS) propagator is by far the easiest to fit, the most consistent results for excited states are obtained there. In Fig. 21 we present the fits for the excited pion, or whatever it is, in the two usual runs.

Often, notably in the case of the $aT_c=\frac{1}{6}$ nucleons, we find that the fitting is made difficult by the fact that the amplitude for the low-mass state is small relative to the excited-state amplitude, and the relative size of the low-mass amplitude seems to decrease as the quark mass decreases. If we examine the four-particle nucleon fits for the $10^3\times 24$, $aT_c=\frac{1}{6}$ lattices we find that for $am_q=0.1$ the amplitudes and masses in the fit to Eq. (5) with $D_{\min}=2$ are 0.0020 and 1.87 for the nucleon and 0.0151 and 2.5 for the excited nucleon (same parity). By the time the quark mass was lowered to 0.025 the amplitude and mass for the nucleon were 0.0004 and 1.39, while for the excited nucleon they were 0.016 and 2.28. The relative size of the corrections to the low-mass particle can be described by the crossover distance, or the distance at which the contributions of the two exponentials are equal. In the case of the two fits above, these distances are about 3.2 and 4.1, respectively. The results for our quenched calculations are similar.

Our pion masses are approximately proportional to $(am_q)^{1/2}$. To make this statement quantitative we fit the pion masses to the form

$$am_\pi = C(am_q)^{1/2} + Dam_q \ , \tag{30}$$

separately for the $aT_c=\frac{1}{4}$ and $\frac{1}{6}$ runs. For the $aT_c=\frac{1}{4}$ runs we find $C=2.728(9)$ and $D=-0.542(31)$, with χ^2 of 0.6 for 1 degree of freedom. The contribution of the term linear in the quark mass is small here, even for the largest quark mass of 0.1, the linear term in the fit contributes -0.05 to the pion mass versus 0.86 for the square-root term. For the $aT_c=\frac{1}{6}$ runs we find $C=3.027(13)$ and $D=-1.313(46)$, with χ^2 of 5.3 for 1 degree of freedom. Here the linear term contributes -0.13 at $am_q=0.1$ versus 0.96 for the square-root term.

TABLE VIII. ρ_2 mass estimates and their confidence levels. We use two-particle fits with $D_{\min}=4$. The notation is the same as Table V.

am_q	$6/g^2$	Small	C.L.	Large	C.L.
0.1	5.525			1.252(17)	0.36
0.05	5.47	0.921(74)	0.79	1.092(49)	0.73
0.025	5.4375	0.841(177)	0.61	0.787(77)	0.32
0.05(V)	5.865			0.831(22)	0.05
0.025(V)	5.865			0.762(45)	0.45

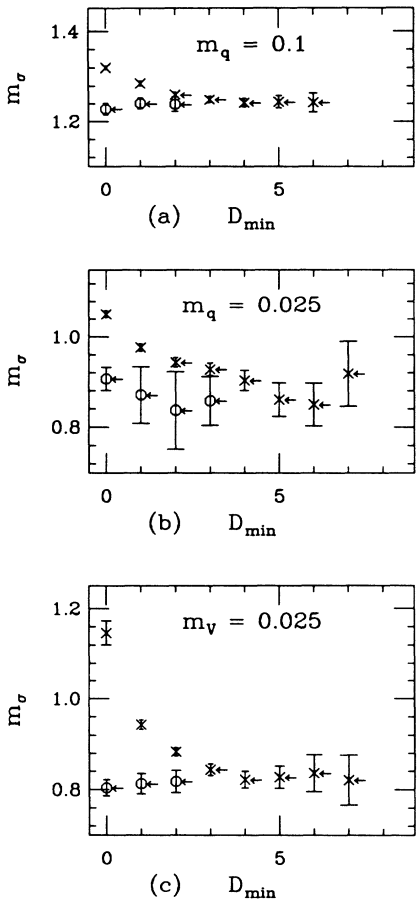

FIG. 16. Fits to the σ mass for the same runs as Fig. 12.

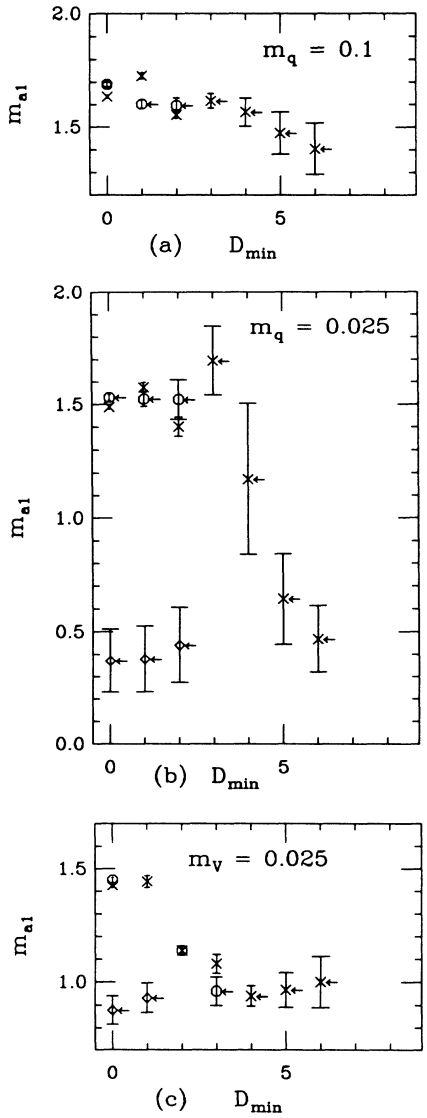

FIG. 17. Fits to the a_1 mass for the same runs as Fig. 12.

The large χ^2 indicates that we need more correction terms to fit the pion mass over this range of am_q for $aT_c=\frac{1}{6}$. This is not surprising, since the physical quark masses are larger for these runs since the lattice spacing is smaller.

If we use these fits to the pion mass together with linear fits to the ρ and N masses as functions of am_q we can estimate the values of am_q at which m_π/m_ρ or m_π/m_N are correct. For $aT_c=\frac{1}{4}$ we find the correct m_π/m_ρ at $am_q=0.0084(6)$ and the correct m_π/m_N at $am_q=0.014(1)$. Similarly, for $aT_c=\frac{1}{6}$ we find $am_q=0.0017(4)$ and 0.0045(3), respectively. The estimates from the ρ and N do not agree because the ρ to N mass ratio is not the physical value in our simulations.

Having estimated the masses we may return to the question of the effects of the spatial-lattice size. Since we have been careful to always use the same fitting form and range on the two lattice sizes, these finite-size effects are somewhat insulated from other systematic errors. Examination of Tables V–XI reveals that any differences between the large and small lattice are small, though it does appear that masses are more often smaller on the larger lattice. The only case where the effect is clear is for the pions, where the masses are quite accurate. Here the average difference in pion mass between the small and large lattices (Table V) is 0.0025(8), where this error can

TABLE IX. σ mass estimates and their confidence levels. We use a three-particle fit with $D_{min}=0$. (The third particle is an excited σ.) The notation is the same as Table V.

am_q	$6/g^2$	Small	C.L.	Large	C.L.
0.1	5.525			1.228(13)	0.88
0.05	5.47	1.095(25)	0.08	1.027(16)	0.85
0.025	5.4375	0.942(25)	0.75	0.906(26)	0.72
0.05(V)	5.865			0.883(15)	0.64
0.025(V)	5.865			0.804(18)	0.63

TABLE X. a_1 mass estimates and their confidence levels. We use a three-particle fit with $D_{min}=1$ for the full QCD runs and $D_{min}=3$ for the quenched runs. Here the third particle is an excited ρ_2. The notation is the same as Table V.

am_q	$6/g^2$	Small	C.L.	Large	C.L.
0.1	5.525			1.601(21)	0.44
0.05	5.47	1.554(40)	0.63	1.507(23)	0.75
0.025	5.4375	1.393(105)	0.70	1.523(32)	0.37
0.05(V)	5.865			1.247(40)	0.26
0.025(V)	5.865			0.960(62)	0.33

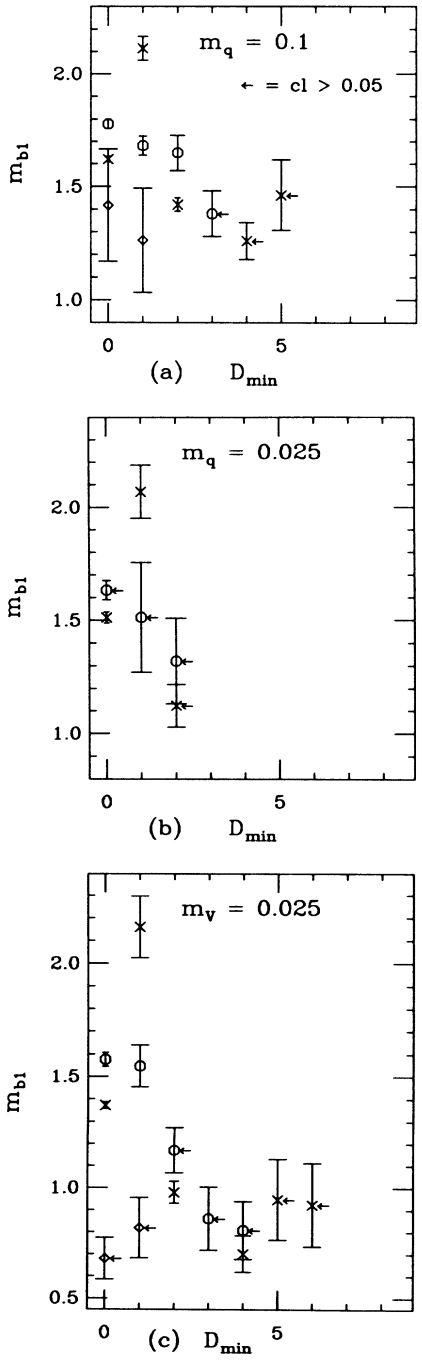

FIG. 18. Fits to the b_1 mass for the same runs as Fig. 12.

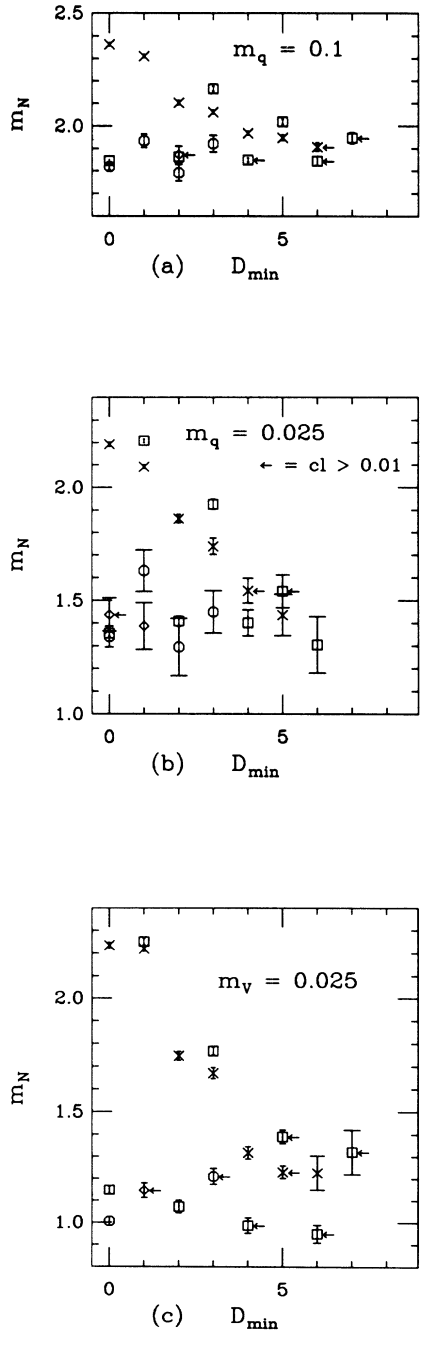

FIG. 19. Fits to the nucleon mass for the same runs as Fig. 12.

TABLE XI. Nucleon mass estimates and their confidence levels. For the $aT_c=\frac{1}{4}$ data we use two-particle fits with $D_{\min}=2$. For the $aT_c=\frac{1}{6}$ data we use one-particle even-distance-only fits with $D_{\min}=4$ for the full QCD runs and $D_{\min}=6$ for the quenched runs. The notation is the same as Table V.

am_q	$6/g^2$	Small	C.L.	Large	C.L.
0.1	5.375			2.273(11)	0.69
0.05	5.32	2.122(218)	0.02	2.193(41)	0.48
0.025	5.2875	1.808(119)	0.85	2.368(315)	0.43
0.1	5.525	1.866(13)	0.38	1.848(10)	0.36
0.05	5.47	1.583(36)	0.74	1.588(27)	0.88
0.025	5.4375	1.571(176)	0.45	1.401(57)	0.002
0.05(V)	5.865			1.200(24)	0.76
0.025(V)	5.865			0.949(40)	0.32

be estimated either from the errors on the individual masses or from the variance of the six differences. Given this, we feel comfortable that our mass results on the larger lattices have only very small effects from the finite spatial size.

There is one striking difference between our results on the small and large lattices—the error bars are generally smaller on the larger lattices. (See Tables V–XI.) We do not know if this is because more lattice sites are averaged in each time slice of the propagator in the larger lattice or because our smaller lattices are occasionally flirting with ordering of the Polyakov loops in the spatial directions. Either way, it appears that we produced results of equal

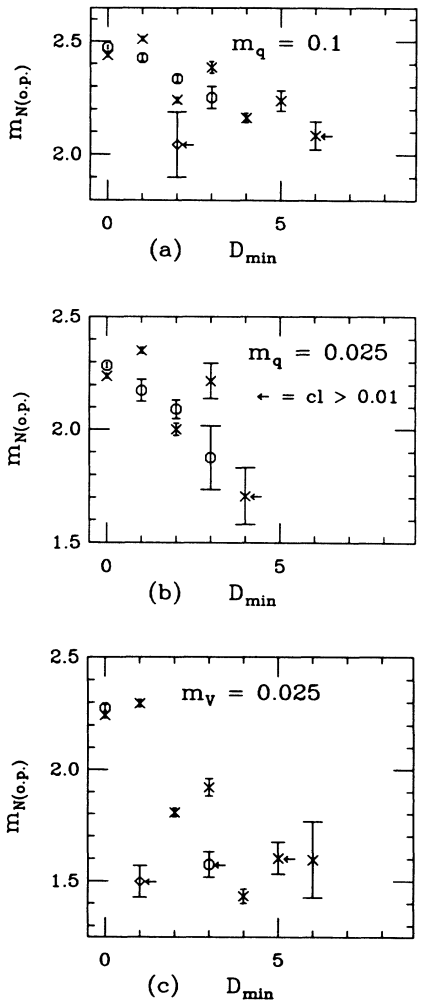

FIG. 20. Fits to the opposite-parity (o.p.) nucleon mass for the same runs as Fig. 12.

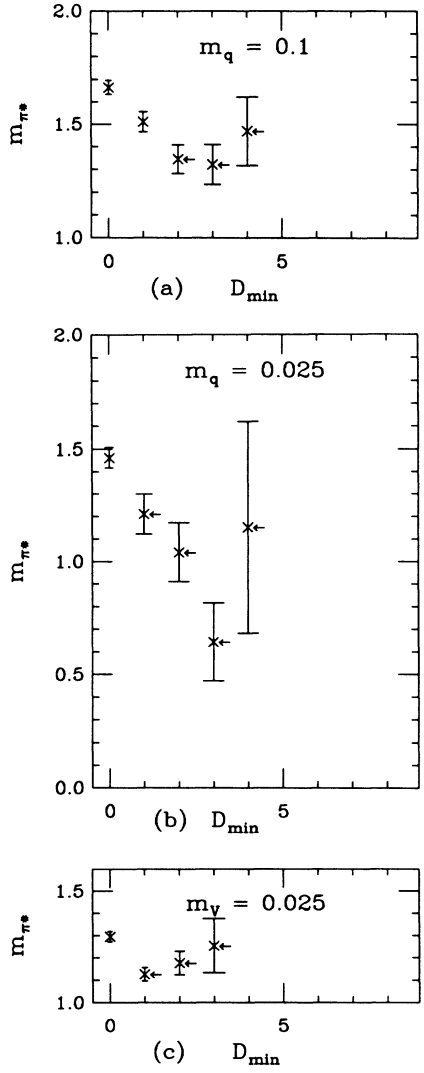

FIG. 21. Fits to the excited π mass for the same runs as Fig. 12.

accuracy on our larger lattices without using more computer time.

There is one respect in which finite lattice size will eventually make a big difference. Many of the particles, such as the ρ, are unstable against decay into two pions. For the ρ and other spin-1 mesons these pions would need nonzero spatial momentum, and the energy of these two-pion states would be dependent on the lattice size. Our lattices are not large enough for such ρ decays to occur. For the σ (0^{++}) channel our $\bar{q}q$ source could be coupling to a two-pion state. Indeed for our lowest-quark mass the σ mass is about twice the pion mass. Because we see no dramatic difference in the amplitude or mass in this propagator at this lowest mass and because the quenched calculation, where a $\bar{q}q$ source cannot couple to two pions, shows similar results in this propagator we think that the correct interpretation of the observed exponential is as a 0^{++} meson.

Several groups have performed spectrum calculations using full QCD (Ref. 17). Two of these other calculations use two flavors of Kogut-Susskind fermions, and it is interesting to compare our results. Billoire and Marinari[23] reported results for the π and ρ masses from a pseudofermion calculation with $am_q=0.1$ and 0.2 on a $6^3\times 12$ lattice (which was doubled in the time direction for the calculation of quark propagators). Their coupling value $6/g^2=5.4$ is close to our stronger coupling of 5.375. To make a direct comparison with their results for $am_q=0.1$ we make a linear interpolation of our mass estimates in our smaller lattices between $6/g^2=5.375$ and 5.525 to estimate a mass at $6/g^2=5.4$. For the pion we find 0.8153(16) while Billoire and Marinari quote 0.819(4). For the ρ we find 1.414(16) and Billoire and Marinari find 1.38(1). Thus these results are in quite reasonable agreement.

A second calculation by Fukugita, Ohta, Oyanagi, and Ukawa[24] used the Langevin method on an $8^3\times 18$ lattice with $6/g^2=5.5$ and quark masses of 0.2, 0.1, and 0.05. For $am_q=0.1$ this coupling falls near our weaker coupling of 5.525, and we can again make a linear interpolation between our two couplings. For $am_q=0.05$ their coupling is smaller than our weaker coupling of $6/g^2=5.47$ so we must make an extrapolation to compare masses. For the pion masses at $am_q=0.1$ and 0.05 Fukugita, Ohta, Oyanagi, and Ukawa find 0.8343(44) and 0.6266(74), respectively. Our interpolated and extrapolated estimates from our $8^3\times 24$ runs are 0.8277(8) and 0.6182(20), respectively. These values are in reasonable agreement considering the possible corrections to our linear interpolation. For the ρ and nucleon the situation is a little more complicated. Fukugita, Ohta, Oyanagi, and Ukawa use two-particle fits with a minimum distance of two. If we interpolate and/or extrapolate the results of our two-particle $D_{\min}=2$ fits to $6/g^2=5.5$ we find 1.299(5) and 1.172(19) for the ρ masses at $am_q=0.1$ and 0.05, while Fukugita, Ohta, Oyanagi, and Ukawa find 1.299(19) and 1.139(45) for the ρ masses at these two-quark masses. Similarly for the nucleon we find 2.141(7) and 1.898(18) while they report 2.119(45) and 1.949(99). These numbers are in good agreement. However, from Figs. 13 and 19 it is apparent that two-particle fits with $D_{\min}=2$ still contain substantial contributions from excited states. Moreover, the confidence levels of these fits are very low—for the $aT_c=\frac{1}{6}$ lattice the confidence levels of these ρ and nucleon fits were 10^{-7}, 0.06, 10^{-40}, and 10^{-9}, respectively. Therefore we have chosen other fits as discussed above, and our reported results for the ρ and nucleon masses are somewhat lower than those of Fukugita, Ohta, Oyanagi, and Ukawa. If we interpolate or extrapolate the fits we actually selected on the $8^3\times 24$ lattices to $6/g^2=5.5$ we find masses of 1.261(18) and 1.075(135) for the ρ at $am_q=0.1$ and 0.05, respectively, and masses of 1.934(11) and 1.461(44) for the nucleon. The confidence levels for these four fits on the $8^3\times 24$ lattices were 0.01, 0.94, 0.38, and 0.74. If we use our $10^3\times 24$ results to interpolate and/or extrapolate to $6/g^2=5.5$ the ρ masses are 1.243(13) and 0.843(55), while the nucleon masses are 1.919(9) and 1.467(33) for the two-quark masses.

V. T_c ESTIMATES

Since our hadron mass estimates were made at a lattice spacing known in units of the chiral-symmetry-restoration temperature, they can be used to estimate the temperature of the symmetry restoration in physical units. This calculation is summarized in Table XII. For each quark mass and coupling, we use our estimate of $6/g^2$ for the chiral-symmetry restoration to compute aT_c in the spectrum run. The errors on our estimate of aT_c are obtained from the error on $6/g_c^2$ and the difference in $6/g_c^2$ for $N_t=4$ and 6. We then use the mass values in Tables VI–XI to estimate T_c in units of MeV, using first the ρ and then the N masses as standards. We also give linear extrapolations of these estimates of T_c to the physical quark masses. Of course we do not expect the ρ and nucleon masses to be independent of am_q, so this estimate of T_c is really only in units of MeV at the extrapolated quark mass. We use this fitting method rather than extrapolating the hadron masses because this method makes it straightforward to include the errors on our estimate of $6/g_c^2$ in the computation. Many quenched spectrum calculations are in the literature and the pure gauge theory deconfinement temperature can be estimated from any of them and the known results[25] for $6/g_c^2$. Figure 22 shows our estimates with dynamical fermions together with a number of T_c estimates from quenched calculations[14,26,8] as a function of inverse lattice spacing. As usual, the quoted errors are statistical only. The full QCD estimates differ slightly from those we reported earlier[9,27] because we have since completed our runs on the hadron spectrum and modified our procedures for selecting a fit. Also, we have slightly changed our estimates of $6/g_c^2$ for $am_q=0.025$ based on recent high-temperature runs at both $aT_c=\frac{1}{4}$ and $\frac{1}{6}$.

A lowering of the chiral-restoration temperature by dynamical quarks is intuitively reasonable. The breaking of chiral symmetry is associated with a clustering of eigenvalues of the fermion hopping matrix around zero.[28] With the determinant in the probability weighting such configurations are suppressed, and it is harder to break chiral symmetry.

TABLE XII. Estimation of the chiral-symmetry-restoration temperature in MeV. The columns are the quark mass, the gauge coupling, the crossover temperature in units of the lattice spacing, and the critical temperatures estimated using the ρ and N masses as standards. Quark masses tagged with "ex" refer to linear extrapolations of the T_c values.

am_q	$6/g_c^2$	aT_c	$T_c(\rho)$	$T_c(N)$
		$aT_c=\frac{1}{4}$		
0.1	5.375(20)	0.250(10)	137(6)	103(4)
0.05	5.320(10)	0.250(05)	137(5)	107(3)
0.025	5.280(10)	0.249(05)	143(6)	99(13)
0.0084(ex)	$\chi^2=0.33$ (1 DF)		142(6)	
0.014(ex)	$\chi^2=0.5$ (1 DF)			109(6)
		$aT_c=\frac{1}{6}$		
0.1	5.525(40)	0.167(22)	106(14)	85(11)
0.05	5.470(40)	0.167(22)	137(19)	99(13)
0.025	5.430(30)	0.166(17)	149(24)	111(12)
0.0018(ex)	$\chi^2=0.008$ (1 DF)		164(25)	
0.0044(ex)	$\chi^2=0.05$ (1 DF)			117(14)
		Quenched		
0.05	5.865(15)	0.167(05)	166(7)	131(5)
0.025	5.865(15)	0.167(05)	200(19)	165(9)
0(ex)	(0 DF)		234(39)	200(18)

VI. CONCLUSIONS

In this calculation of hadron masses in full QCD we have attempted to carefully control systematic errors. By running at two different lattice sizes we have empirically checked the effect of the spatial size of the lattice, and by fitting the propagators over many distance ranges we have checked the effect of temporal-lattice size and excited states in the propagators. We emphasize the importance of propagator fitting procedures, and describe ours in some detail.

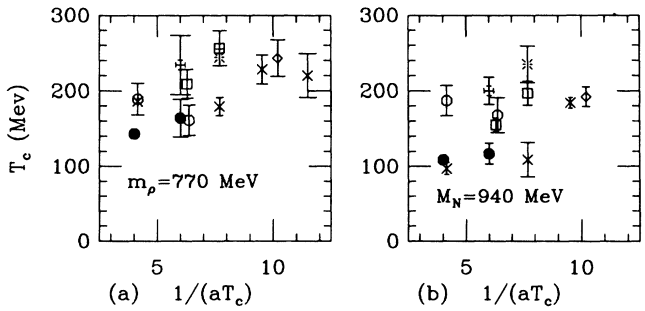

FIG. 22. T_c estimates using (a) the ρ mass and (b) the nucleon mass as a standard for the deconfinement (pure gauge) transition and for the chiral-symmetry-restoration (full QCD) transition. The abscissa corresponds to the number of time slices at T_c. The filled circles are our estimates for two flavors of dynamical quarks. For the pure gauge theory the crosses are Bowler, Chalmers, Kenway, Pawley, and Roweth (Ref. 14) and Bowler, Chalmers, Kenway, Roweth, and Stephenson (Ref. 8), the open circles Gilchrist, Schierholz, Schneider, and Teper (Ref. 22) and Gilchrist, Schneider, Schierholz, and Teper (Ref. 26), the diamonds Gupta, Guralnik, Kilcup, Patel, Sharpe, and Warnock (Ref. 8), the stars Hamber (Ref. 26), and the squares Campostrini, Moriarty, Potvin, and Rebbi (Ref. 26). The fancy plus is our quenched calculation.

The familiar problem of the too large nucleon to ρ mass ratio is present in our results. On our $10^3\times 24$ $aT_c=\frac{1}{6}$ lattices we find N/ρ mass ratios of 1.53(2), 1.71(9), and 1.70(19) for quark masses of 0.1, 0.05, and 0.025, respectively. In these ratios we include correlations between the N and VT propagators as described in Sec. II, using the same minimum distances for the ρ and nucleon as in the individual particle mass estimates. It remains uncertain whether the solution to this problem is smaller lattice spacing, smaller quark mass, simulations on lattice sizes such that the ρ really can decay, or some combination of these.

It is apparent from the simple fact that our hadron masses are about one in units of a^{-1} that we are nowhere near the continuum limit in this calculation and that it is important to move to smaller lattice spacing. Another indication of this is the fact that while our π masses are going to zero with am_q as expected, our π_2 masses are close to the other mesons. It is interesting to note that this situation is much better in our quenched calculation. This full QCD simulation is approaching but has not reached the point where particle decays, or the presence of multiparticle states, must be considered.

Generally our $aT_c=\frac{1}{6}$ quenched calculation appears to be closer to the continuum limit than our $aT_c=\frac{1}{6}$ full QCD calculation, as evidenced by the generally smaller hadron masses and the smaller violations of flavor symmetry in the quenched calculation. If the hadron masses are chosen to define the mass scale in quenched QCD, this leads to the conclusion that the temperature of the phase transition in quenched QCD is significantly higher than in full QCD.

ACKNOWLEDGMENTS

We would like to thank C. Bernard, P. Mackenzie, E. Marinari, J. McCarthy, and D. Sinclair for helpful con-

versations. We thank M. Fukugita for providing details of their results. This work was supported in part by National Science Foundation Grants Nos. PHY-86-14185 and DMR83-20423, and by Department of Energy Grants Nos. DE-AT03-81ER40029 and DE-AC02-84ER-40125. We are grateful to E. I. DuPont de Nemours Co., Star Technologies Inc., and Xerox Corporation for their support. D.T. thanks the Alfred P. Sloan Foundation for financial support. S.G. would like to thank Fermilab for its hospitality.

[1]M. Creutz, Phys. Rev. Lett. **43**, 553 (1979).

[2]H. Hamber and G. Parisi, Phys. Rev. Lett. **47**, 1792 (1981); E. Marinari, G. Parisi, and C. Rebbi, *ibid.* **47**, 1975 (1981); D. Weingarten, Phys. Lett. **109B**, 57 (1982).

[3]S. Gottlieb, P. B. Mackenzie, H. B. Thacker, and D. Weingarten, Phys. Lett. **134B**, 346 (1984); Nucl. Phys. **B263**, 704 (1986).

[4]S. Gottlieb, in *Advances in Lattice Gauge Theory,* proceedings of the Tallahassee Conference, Florida State University, 1985, edited by D. W. Duke and J. F. Owens (World Scientific, Singapore, 1985); H. B. Thacker, *ibid.*

[5]R. C. Brower, M. B. Gavela, R. Gupta, and G. Maturana, Phys. Rev. Lett. **53**, 1318 (1984); N. Cabibbo, G. Martinelli, and R. Petronzio, Nucl. Phys. **B244**, 381 (1984); C. Bernard, in *Gauge Theory on a Lattice: 1984,* edited by C. Zachos, W. Celmaster, E. Kovacs, and D. Sivers (Argonne National Laboratory, Argonne, 1984).

[6]For a recent review, see M. Fukugita, in *Lattice Gauge Theory Using Parallel Processors,* proceedings of the CCAST Symposium, 1987, edited by X. Li, Z. Qiu, and H. Ren (Gordon and Breach, London, 1987).

[7]H. Kluberg-Stern, A. Morel, O. Napoly, and B. Petersson, Nucl. Phys. **B220**, 447 (1983).

[8]K. C. Bowler, C. B. Chalmers, R. D. Kenway, D. Roweth, and D. Stephenson, Nucl. Phys. **B296**, 732 (1988); R. Gupta, G. Guralnik, G. Kilcup, A. Patel, S. R. Sharpe, and T. Warnock, Phys. Rev. D **36**, 2813 (1987).

[9]S. Gottlieb, W. Liu, D. Toussaint, R. L. Renken, and R. L. Sugar, Phys. Rev. Lett. **59**, 1513 (1987).

[10]H. C. Andersen, J. Chem. Phys. **72**, 2384 (1980); S. Duane, Nucl. Phys. **B257**, 652 (1985); S. Duane and J. Kogut, Phys. Rev. Lett. **55**, 2774 (1985).

[11]S. Gottlieb, W. Liu, D. Toussaint, R. L. Renken, and R. L. Sugar, Phys. Rev. D **35**, 2531 (1987).

[12]F. Fucito and S. Solomon, Phys. Lett. **140B**, 387 (1984).

[13]See Kluberg-Stern, Morel, Napoly, and Petersson (Ref. 7); J. Gilchrist, H. Schneider, G. Schierholz, and M. Teper, Nucl. Phys. **B248**, 29 (1984); A. Morel and J. Rodrigues, *ibid.* **B247**, 44 (1984); A. Billoire, R. Lacaze, E. Marinari, and A. Morel, *ibid.* **B251**, 581 (1985).

[14]K. C. Bowler, C. B. Chalmers, R. D. Kenway, G. S. Pawley, and D. Roweth, Nucl. Phys. **B284**, 299 (1987).

[15]T. A. DeGrand, Phys. Rev. D **36**, 176 (1987); C. DeTar and J. B. Kogut, *ibid.* **36**, 2828 (1987).

[16]S. Gottlieb, W. Liu, D. Toussaint, R. L. Renken, and R. L. Sugar, Phys. Rev. D **35**, 3972 (1987).

[17]For a review of this literature see M. Fukugita, Nucl. Phys. B Proc. Suppl. **4**, 105 (1988).

[18]G. Martinelli, G. Parisi, R. Petronzio, and F. Rapuano, Phys. Lett. **122B**, 283 (1983); R. Gupta and A. Patel, *ibid.* **124B**, 94 (1983); Nucl. Phys. **B226**, 152 (1983).

[19]For an early review, see B. Svetitsky, in *Gauge Theory on a Lattice: 1984* (Ref. 5).

[20]Ph. de Forcrand, K.-H. Mütter, K. Schilling, and R. Somer, in *Lattice Gauge Theory '86,* proceedings of the Lattice Gauge Theory Conference, Upton, New York, 1986, edited by H. Satz, I. Harrity, and J. Potvin (NATO ASI Series B, Vol. 159) (Plenum, New York, 1987).

[21]S. Gottlieb, W. Liu, D. Toussaint, R. L. Renken, and R. L. Sugar, Phys. Rev. D **36**, 3797 (1987).

[22]J. P. Gilchrist, G. Schierholz, H. Schneider, and M. Teper, Nucl. Phys. **B248**, 29 (1984).

[23]A. Billoire and E. Marinari, Phys. Lett. B **184**, 381 (1987).

[24]M. Fukugita, S. Ohta, Y. Oyanagi, and A. Ukawa, Phys. Lett. B **191**, 164 (1987).

[25]A. D. Kennedy, J. Kuti, S. Meyer, and B. J. Pendleton, Phys. Rev. Lett. **54**, 87 (1985); S. A. Gottlieb, A. D. Kennedy, J. Kuti, S. Meyer, B. J. Pendleton, R. L. Sugar, and D. Toussaint, *ibid.* **55**, 1958 (1985); N. H. Christ and A. E. Terrano, *ibid.* **56**, 111 (1985); D. Toussaint, S. A. Gottlieb, A. D. Kennedy, J. Kuti, S. Meyer, B. J. Pendleton, and R. L. Sugar, in *Lattice Gauge Theory '86* (Ref. 20).

[26]See Bowler, Chalmers, Kenway, Pawley, and Roweth (Ref. 14); J. P. Gilchrist, H. Schneider, G. Schierholz, and M. Teper, Phys. Lett. **136B**, 87 (1984); H. Hamber, Nucl. Phys. B (to be published); M. Campostrini, K. J. M. Moriarty, J. Potvin, and C. Rebbi, Phys. Lett. B **193**, 79 (1987).

[27]S. Gottlieb, W. Liu, D. Toussaint, R. L. Renken, and R. L. Sugar, Nucl. Phys. B Proc. Suppl. **4**, 155 (1988).

[28]I. M. Barbour, P. Gibbs, J. P. Gilchrist, H. Schneider, G. Schierholz, and M. Teper, Phys. Lett. **136B**, 80 (1984).